Fuel 299 (2021) 120523

Contents lists available at ScienceDirect

Fuel

journal homepage: www.elsevier.com/locate/fuel

Full Length Article

Influence of pressure on the gasification kinetics of two high-temperature beech wood chars with CO_2, H_2O and its mixture

Christoph Schneider [a,*], Michael Zeller [b], Daniel Böhm [a], Thomas Kolb [a,b]

[a] Karlsruhe Institute of Technology, Engler-Bunte-Institute, Fuel Technology, EBI-ceb, Engler-Bunte-Ring 3, 76131 Karlsruhe, Germany
[b] Karlsruhe Institute of Technology, Institute for Technical Chemistry, ITC, Hermann-von-Helmholtz-Platz 1, 76344 Eggenstein-Leopoldshafen, Germany

ARTICLE INFO

Keywords:
Biomass char
Gasification kinetics
CO_2/H_2O partial pressure
Total pressure
Single-particle reactor
Forced flow-through conditions

ABSTRACT

This paper presents experimental data and modeling approaches to describe the influence of CO_2 and H_2O partial pressure as well as absolute pressure on the gasification kinetics of two different beech wood chars. The chars were produced at 1400 °C (P1400) and 1600 °C (P1600) at high-heating rates and short residence times in a drop-tube reactor. The gasification experiments were conducted in a single-particle reactor with forced flow-through conditions reducing diffusional effects to a minimum. The interpretation of the experimentally determined reaction rates during gasification with CO_2, H_2O and its mixture is based on the char properties (graphitization, ash dispersion and morphology) presented in a previous publication.

During gasification with CO_2, P1600 shows higher reactivity as compared to P1400 for all CO_2 partial pressures and temperatures applied. The higher reactivity of P1600 during CO_2 gasification may be explained by a CaO film on the char surface catalyzing the char-CO_2 gasification reaction. On the other hand, P1400 shows higher reactivity towards H_2O which may be evoked by the lower graphitization degree and higher specific surface area. Reaction kinetic modeling for single atmosphere gasification was successfully carried out using a power law approach. The Langmuir-Hinshelwood model, however, only gave good results where a possible saturation of the char surface at high pressure was observed.

Increasing the CO_2 partial pressure during gasification in mixed CO_2/H_2O atmospheres leads to higher reactivity for both chars. The reaction rate r_{mix} can be expressed by addition of the single atmosphere reaction rates in the low pressure area suggesting a separate active site mechanism. Catalytic activity of CaO increases the P1600 reactivity distinctively for lower H_2O and CO_2 partial pressures. For higher H_2O and CO_2 partial pressures, P1600 reactivity stagnates due to lower specific surface area and higher graphitization degree. Here, a common active sites mechanism can be assumed.

1. Introduction

The use of low-grade biogenic and fossil fuels in high-pressure entrained-flow gasification (EFG) allows for the production of high-quality synthesis gas that can be converted into fuels and chemicals or used for power generation via integrated gasification combined cycle (IGCC) systems. In the near future, EFG can play an important role in satisfying the demand for basic chemicals and power [1,2]. In EFG, the fuel is converted via thermal and thermo-chemical processes i.e. drying, pyrolysis under high heating rates as well as the subsequent heterogeneous gasification reactions of the resulting char in a CO_2– and H_2O-rich atmosphere. For the achievement of a high cold gas efficiency, a complete char conversion is desired. Since the heterogeneous reactions are considered as the rate-limiting step for complete fuel conversion, the knowledge of the gasification kinetics is essential for the design of entrained-flow gasifiers [3].

The heterogeneous gasification of char particles is controlled by process parameters, i.e. temperature, partial pressure of the reactant gas and process pressure as well as the chemical and physical properties of the char. Char properties affecting the conversion rate during gasification mainly include surface area and porosity, graphitization of the carbon matrix and inorganic ash components [4–8]. Generally, the heterogeneous char gasification reactions with CO_2 and H_2O can be described by an oxygen exchange mechanism [9]. In the case of CO_2 gasification, the following reaction mechanism presented in (R1)–(R3) is widely accepted [9,10].

* Corresponding author.
E-mail address: ch.schneider@kit.edu (C. Schneider).

https://doi.org/10.1016/j.fuel.2021.120523
Received 20 November 2020; Received in revised form 16 February 2021; Accepted 18 February 2021

$$C_f + CO_2 \xrightarrow{k_1} C(O) + CO \quad (R1)$$

$$C(O) + CO \xrightarrow{k_2} C_f + CO_2 \quad (R2)$$

$$C(O) \xrightarrow{k_3} CO \quad (R3)$$

Here, C_f represents an active site on the char surface and C(O) a carbon oxygen intermediate while $k_{1\text{-}3}$ are Arrhenius rate constants. As can be seen from (R2), the presence of CO exerts an inhibitory effect by lowering the concentration of the C(O) carbon oxygen intermediate. If a steady-state assumption is applied and the rate of reaction is described by the rate of desorption of the carbon oxygen intermediate (R3), the following Langmuir-Hinshelwood (LH) approach can be used [9].

$$r_{CO_2}(T, p_{CO_2}, p_{CO}) = \frac{k_1 p_{CO_2}}{1 + \frac{k_2}{k_3} p_{CO} + \frac{k_1}{k_3} p_{CO_2}} \quad (1)$$

For low CO concentrations, the inhibitory effect of CO is negligible and CO partial pressure p_{CO} can be set to zero [11]. Furthermore, a simplified global kinetic model can also be applied (see Eq. (2)).

$$r_{CO_2}(T, p_{CO_2}) = k_{0,CO_2} \exp\left(-\frac{E_{A,CO_2}}{R_U T}\right) p_{CO_2}^{n_{CO_2}} \quad (2)$$

Here, k_{0,CO_2} represents the pre-exponential factor, E_{A,CO_2} the activation energy, R_U the universal gas constant, T the reaction temperature and n_{CO_2} the reaction order towards CO_2 partial pressure.

The reaction of carbon with steam proceeds similarly to the Boudouard reaction but has more possible inhibition steps as summarized by Hüttinger & Merdes [12].

$$C_f + H_2O \xrightarrow{k_4} C(O) + H_2 \quad (R4)$$

$$C(O) + H_2 \xrightarrow{k_5} C_f + H_2O \quad (R5)$$

$$C(O) \xrightarrow{k_6} CO \quad (R6)$$

$$C_f + H_2 \xrightarrow{k_7} C(H_2) \quad (R7)$$

$$C(H_2) \xrightarrow{k_8} C_f + H_2 \quad (R8)$$

$$C_f + \frac{1}{2} H_2 \xrightarrow{k_9} C(H) \quad (R9)$$

$$C(H) \xrightarrow{k_{10}} C_f + \frac{1}{2} H_2 \quad (R10)$$

Basically, the reaction steps can be subsumed into two main processes: the oxygen exchange mechanism (see (R4)–(R6)) and possible hydrogen inhibition reactions (see (R7) to (R10)). Again, $k_{4\text{-}10}$ are Arrhenius rate constants while C(H) and $C(H_2)$ represent carbon hydrogen intermediates. Hydrogen not only inhibits the reaction by lowering the amount of C(O) carbon oxygen intermediates (see (R5)) but also by direct adsorption on carbon active sites C_f associatively (see (R7)) or dissociatively (see (R9)). However, the experimental data presented within this work was obtained in a simplified system containing very low amounts of product gases. Thus, this paper focusses on the oxygen exchange mechanism (see (R4)–(R6)) while inhibitory effects via adsorption of H_2 were not explicitly investigated leading to a simplified rate expression (see Eq. (3)). This approach is also consistent with previous experimental studies where kinetic data for the carbon steam reaction is determined [11,13].

$$r_{H_2O}(T, p_{H_2O}, p_{H_2}) = \frac{k_4 p_{H_2O}}{1 + \frac{k_5}{k_6} p_{H_2} + \frac{k_4}{k_6} p_{H_2O}} \quad (3)$$

Again, for low H_2 concentrations, the inhibitory effect of H_2 is negligible and H_2 partial pressure p_{H_2} can be set to zero [11]. Thus, a simplified global kinetic model is applicable as well (see Eq. (4)).

$$r_{H_2O}(T, p_{H_2O}) = k_{0,H_2O} \exp\left(-\frac{E_{A,H_2O}}{R_U T}\right) p_{H_2O}^{n_{H_2O}} \quad (4)$$

k_{0,H_2O} represents the pre-exponential factor, E_{A,H_2O} the activation energy and n_{H_2O} is the reaction order towards H_2O partial pressure for the carbon steam reaction.

In a technical entrained-flow gasifier, CO_2 and H_2O always coexist in the syngas produced. Thus, knowledge about the dominating heterogeneous gasification reaction when both gases are present is required. According to publications investigating the gasification kinetics of char in mixed atmospheres of CO_2 and H_2O, two possible surface reaction mechanisms were proposed.

The first mechanism accounts for the existence of active sites that are suitable for both char-CO_2 and char-H_2O reaction [4,14–18]. Thus, CO_2 and H_2O are competing for the same active sites inhibiting each other. Roberts & Harris [14] investigated the gasification of three Australian bituminous coal chars in mixtures of CO_2 and H_2O in a thermogravimetric analyzer (TGA) at elevated pressure up to 50 bar. Their data indicate that the gasification rate in a mixture of CO_2 and H_2O did not add up to the sum of the two pure-gas reaction rates. Thus, they proposed a kinetic equation to interpret their experimental data based on the assumption that both reactions compete for the same active sites. Chen et al. [17] investigated the effect of pyrolysis conditions on char gasification with mixtures of CO_2 and H_2O in a TGA and a fluidized-bed reactor using two differently pyrolyzed lignite chars (fast and slow pyrolysis). The authors report that the char gasification rates in the mixture of CO_2 and H_2O were lower than the sum of the rates of the char reacting independently with CO_2 and H_2O. However, the reaction rates in the mixed atmospheres were higher than the rate of each independent reaction for both the fast pyrolysis and slow pyrolysis char gasification. Furthermore, their results from TGA and fluidized-bed indicate that the char-H_2O reaction was independent of the char-CO_2 reaction, while the char-CO_2 reaction was inhibited by the char-H_2O reaction.

An alternative reaction mechanism for the gasification of chars in mixtures of CO_2 and H_2O is based on the assumption that the char-CO_2 and the char-H_2O reactions occur at separate active sites [19–23]. Guizani et al. prepared beech wood chars at low [21] and high heating rate [23] and found that the beech wood char reactivity is fairly represented by this additive approach for temperatures up to 900 °C and relatively low reactant partial pressures. Gasification experiments in mixtures of CO_2 and H_2O at elevated pressure using a fixed-bed reactor were carried out by Li et al. [22]. Their results indicate that the dominating reaction mechanism depends on the total pressure applied. They conclude that under low reactant pressures, the reaction mechanism was consistent with the separate reactive site reaction mechanism, while under higher pressure, the common active site reaction mechanism is rather valid. A short literature review concerning biomass, lignite and coal char gasification in mixed atmospheres is conducted by Guizani et al. [21], the quintessence being that no conclusive statement is possible whether the two reactions are competing or additive.

In literature, a vast amount of kinetic data for the gasification of fossil [24] and biogenic [25] fuels with both CO_2 and H_2O is available. However, the kinetic parameters may vary several orders of magnitude depending on the fuel, the char particle size, the experimental set-up used and the pyrolysis conditions applied. Pyrolysis conditions affect graphitization degree of the carbon matrix [26,27], char morphology [28,29] and dispersion of inorganic ash components [30,31]. In a previous publication [32], the authors were able to show an effect of both ash dispersion and graphitization on the gasification rate with CO_2. The investigated beech wood char samples were pyrolyzed in a drop-tube reactor under high heating rates, short residence times and temperatures between 1000 °C and 1600 °C in order to imitate the process conditions found in technical entrained-flow gasifiers. Due to thermal stress during pyrolysis, an increasing graphitization of the carbon matrix

leads to a decrease in initial conversion rate R_0 during gasification with CO_2. However, a thin layer of CaO that formed on the char surface at a pyrolysis temperature of 1600 °C was found to significantly increase the conversion rate of the char-CO_2 reaction.

Furthermore, the experimental set-up may have impact on the kinetic data obtained. The thermogravimetric analyzer (TGA) is most widely used for the determination of gasification kinetics of fossil and biogenic solid fuels [24,25]. However, diffusional effects due to the limited gas flow through the char sample may evoke artefacts. These artefacts would lead to observed reaction rates that are not truly intrinsic but rather a superposition of diffusion processes and the chemical reaction. Diffusion of the reactant gas through the crucible freeboard and the char bed must be taken into consideration in order to verify the kinetic data obtained [33,34]. Therefore, the experimental process parameters i.e. sample mass, temperature, gas velocity and reactant partial pressure must be carefully chosen when using TGA in order to determine kinetic data that are truly intrinsic [35]. It is important to conduct intrinsic gasification experiments in a TGA at relatively low temperatures in order to ensure that the diffusion processes are always faster than the actual gasification reaction. Especially for highly reactive bio-chars, the process window for the determination of intrinsic reaction rates during gasification is narrow in a TGA. Additionally, when higher pressures are applied in a TGA, even more restrictions may occur. Diffusion coefficients are inversely proportional to pressure ($D_{AB} \sim 1/p$). Furthermore, the maximum gas flow rate of a TGA is usually below 1 l/min at standard ambient temperature and pressure (rather around 50–200 ml/min). Increasing the pressure in a TGA leads to a proportional decrease of gas velocity towards the crucible as the volume flow rate at standard ambient temperature and pressure cannot be further increased. Moreover, high reactant gas volume flows during pressurized TGA experiments lead to a lot of noise in the mass signal.

Other experimental concepts such as vertically blown reactors (e.g. fixed-bed reactors) may be more suitable for the determination of gasification kinetics allowing for the application of wider process parameter windows. Here, the reactant gas is forced to flow through the char sample ameliorating mass transport of educt gas to and removal of product gas from the sample. Wu & Wang [36] investigated the effect of pressure on the K_2CO_3-catalyzed steam gasification of ash-free coal in a vertically blown reactor. The experimental set-up was operated as a differential reactor applying steam partial pressures of up to 6 bar and total pressures of 20 bar. The authors state that diffusional effects can be eliminated thoroughly by this type of reactor. Furthermore, kinetic parameters using an nth-order and a LH approach were determined.

From literature review it becomes obvious that kinetic data for pressurized gasification of biogenic char generated under typical EFG conditions (high heating rate, short residence time and high temperature) is rather scarce. For the determination of gasification kinetics at elevated pressure, a TGA is often used where the elimination of diffusional effects is difficult to be achieved, especially for highly reactive biogenic chars. Furthermore, gasification kinetics for bio-chars using CO_2, H_2O and its mixture at elevated pressure has not been investigated extensively to the best of our knowledge. Concerning the dominating reaction mechanism during gasification of bio-chars in mixtures of CO_2 and H_2O, no conclusive statement about the interdependence of the two reactions was found in literature.

The aim of this work is to determine the influence of pressure on the gasification kinetics for two beech wood chars that were produced under inert conditions at 1400 °C and 1600 °C at high-heating rates and short residence times in a drop-tube reactor imitating the conditions found during EFG. These chars exhibited different reactivities towards CO_2 due to distinct differences in morphology, graphitization and catalytic influence of ash components arising from their various pyrolysis temperatures [32]. The gasification experiments presented in this work are conducted in a single-particle reactor with forced flow-through conditions reducing diffusional effects to a minimum. The reactant gases flow convectively through the char particles. It was assured that the reactor was operated in a differential way meaning that the reactant gas concentration did not decrease >3 vol-% along the particle bed. Thus, all char particles were able to get in contact with the desired gas concentration and no concentration gradient was formed. Furthermore, the gas velocity was kept constant at a high level. Consequently, no accumulation of product gas near the char particles occurred as it may happen at the bottom of a TGA crucible. Since the product gas is swept away by the gas flow convectively, re-adsorption of product gases on the char surface is minimized. Product gas re-adsorption could possibly inhibit the gasification reaction leading to observed reaction rates that are not truly intrinsic. The interpretation of the experimentally determined reaction rates during gasification with CO_2, H_2O and its mixture is based on the char properties (graphitization, ash dispersion and morphology) presented in a previous publication [32]. Kinetic parameters for the gasification of both beech wood chars (P1400 and P1600) with CO_2 and H_2O at elevated pressure are derived using an nth-order as well as a LH approach. Moreover, gasification experiments in a mixture of CO_2 and H_2O are carried out in order to further clarify the dominating reaction mechanism during gasification of biomass chars in CO_2/H_2O containing atmospheres. A possible approach for the reaction kinetic modeling in mixtures of CO_2 and H_2O is presented for both bio-chars.

2. Materials and methods

2.1. Fuel

Commercially available primary beech wood char (Holzkohleverarbeitung Schütte GmbH & Co. KG) was purchased and used as precursor for the secondary pyrolysis experiments in the drop-tube reactor since the same char is utilized in the bioliq® EFG for research operation. The feedstock which is fed into the entrained flow gasifier of the bioliq® process is a suspension fuel consisting of bio-char and pyrolysis oil. The primary char is produced under mild conditions at an estimated pyrolysis temperature of 500–600 °C. Table 1 shows the proximate/ultimate analysis and the micropore surface area of the primary char. It still contains approx. 12 wt-% of volatiles and consists of 1.8 wt-% ash and 85.5 wt-% fixed carbon. Furthermore, the organic components consist of approx. 90 wt-% carbon, 3 wt-% hydrogen and 7 wt–% oxygen (by difference). The micropore surface area was determined with CO_2 at 0 °C and constitutes 394.6 $m^2\ g^{-1}$. For secondary pyrolysis in the drop-tube reactor, the primary char was sieved to a particle fraction of 50–150 µm.

The determination of kinetic parameters was carried out using two secondary chars produced at 1400 °C and 1600 °C in a drop-tube reactor with a residence time of 200 ms. Prior to the analyses and gasification experiments, the secondary chars were sieved to a particle fraction of 50–100 µm. Table 2 shows proximate/ultimate analysis and the micropore surface area of the secondary chars P1400 and P1600. Both chars consist almost of pure carbon with values for fixed carbon of 95.4 wt-% for P1400 and 97.1 wt-% for P1600. Total ash content of both chars is similar, whereas volatile content of P1400 being 2.5% is almost double as compared to P1600. Both chars differ significantly in micropore

Table 1
Properties of primary char.

Proximate analysis / wt.-%, ad	
Moisture	0.9
Ash content	1.8
Volatiles	11.8
Fixed carbon	85.5
Ultimate analysis / wt.-%, daf	
C	89.8
H	2.6
O (diff)	7.2
N	0.4
Micropore surface area / $m^2\ g^{-1}$	394.6

Table 2
Properties of secondary chars P1400 and P1600.

	P1400	P1600
Proximate analysis / wt.-%, ad		
Moisture	0.2	0.0
Ash content	1.9	1.6
Volatiles	2.5	1.3
Fixed carbon	95.4	97.1
Ultimate analysis / wt.-%, daf		
C	97.2	99.0
H	0.2	0.2
O (diff)	1.9	0.3
N	0.7	0.5
Micropore surface area / $m^2\ g^{-1}$	660.0	126.4

surface area with values of 660.0 $m^2\ g^{-1}$ for P1400 and 126.4 $m^2\ g^{-1}$ for P1600 that can be traced back to a collapse of micropore structure at 1600 °C.

Table 3 shows the ash elemental analysis for both secondary chars determined by inductively coupled plasma optical emission spectrometry (ICP-OES). The main ash component of these beech wood chars is calcium with values between 35.30 wt-% and 39.10 wt-%. A decrease of magnesium content from 1400 °C to 1600 °C can be observed being only 1 wt-% at 1600 °C. For the secondary chars, K/Si ratios are 2.2 and 2.1, respectively while K/(Si + P) ratios have a value of 1.3 being comparatively low (P content of primary char was not determined). Thus, a deactivation of K by Si and P can be assumed [37,38].

In order to gain a better understanding for the experimental results presented in this work, a key figure from our previous publication [32] is shown. In Fig. 1, the most important char characteristics being the initial conversion rate R_0 during gasification with CO_2, CaO dispersion D_{CaO} and graphitization defined as $L_a\ L_{a,0}^{-1}$ are summed up in one graph. Quantification of the CaO dispersion was carried out in a TGA using temperature-programmed reaction (TPR) and chemisorption of CO_2 on CaO at 300 °C. At 300 °C, CO_2 reacts with the CaO atoms on the surface of ash particles forming $CaCO_3$. Increasing the temperature would lead to the carbonization of bulk CaO due to diffusion of CO_2 into the ash particle [39]. Thus, chemisorption of CO_2 at 300 °C can be used to determine the outer surface of CaO particles in the bio-char ash giving a value for the dispersion of CaO particles in mole surface CaO per gram char. The radial expansion of graphene layers of the secondary chars L_a as well as the radial expansion of graphene layers of the primary char $L_{a,0}$ was determined using X-ray diffraction (XRD) and Scherrer equation. Further information about the analyses and methods for char characterization can be found in our previous publication [32]. Concerning the gasification experiments with CO_2, Fig. 1 shows a linear decrease in initial conversion rate R_0 for chars produced at pyrolysis temperatures between 1000 °C and 1400 °C. However, a strong increase of R_0 at a pyrolysis temperature of 1600 °C was encountered. Micropore surface area of the secondary chars showed no correlation with the initial conversion rate R_0 during gasification with CO_2. Graphitization of the carbon matrix suggested the growth of aromatic clusters and graphite-like structures for increasing pyrolysis temperatures up to 1600 °C. Furthermore, CaO dispersion decreased steadily between 1000 °C and 1400 °C whereas a strong increase can be observed at 1600 °C, which is in good accordance with the development of the initial conversion rate R_0 as a function of pyrolysis temperature. Furthermore, SEM/TEM images indicate the formation of a thin CaO layer at 1600 °C that is presumably responsible for the strong increase in initial conversion rate R_0 during gasification with CO_2 (not shown in this work).

Table 3
Ash elemental analysis of primary and secondary chars.

Element	Primary char	P1400C_200ms wt.-%	P1600C_200ms
Ca	38.20	35.30	39.10
K	4.62	5.48	5.05
Mg	6.03	5.80	1.03
Si	2.01	2.51	2.45
P	n. a.	1.73	1.52
Na	0.82	0.96	0.84
Fe	0.74	0.84	0.83
Al	0.25	0.28	0.31

2.2. Pressurized single-particle reactor

Gasification experiments were conducted in a pressurized single-particle reactor that was operated in a differential way allowing only for very low changes in the educt gas phase composition. A schematic flow diagram of the reactor system is shown in Fig. 2. The gas dosing system consists of mass flow controllers (MFC, EL-FLOW, Bronkhorst High-Tech B.V.) for CO_2 and argon allowing for volume flows up to 20 l min^{-1}. Furthermore, one MFC is used for dosing small amounts of nitrogen that is used as a tracer in the analytic strand. Demineralized water is stored in a vessel ($V = 1$ l) and pressurized with 30 bar helium. Measurement of the liquid water flow is carried out using a *mini CORI-FLOW* (Bronkhorst High-Tech B.V.). Steam is generated in a *Controlled Evaporation and Mixing* unit (CEM, Bronkhorst High-Tech B.V.) and - together with a carrier gas - led to the reaction line. A 4-port 2-position valve (V1, VICI) allows the feed gas mixture which is normally entering the reactor to be switched to the bypass line. With this arrangement, the reactor line including the reactor can be purged with argon. The tubular reactor (1200 mm height, 19.5 mm inner diameter) is mounted vertically and can be operated at a pressure of up to 24 bar. The pressure of reaction and bypass line is controlled by back pressure regulators (EL-PRESS, Bronkhorst High-Tech B.V.). Another 4-port 2-position valve (V2, VICI) after the back pressure regulators allows the product gases to either be analyzed using infrared photometry (IR, URAS, ABB) and micro gas chromatography (490 Micro GC, Agilent Technologies) or directly be sent to the off-gas system.

The char is fed into the reactor batch-wise with a dosing unit that is schematically depicted in Fig. 3A. The central component of this device is a brass cylinder (a) with a cylindrical bore where the char is placed prior to the gasification experiment. This brass cylinder can be removed from the dosing unit in order to fill the bore with char and weigh the sample. When the brass cylinder (a) is inserted into the dosing unit, it is sealed with PTFE foil. The brass cylinder (a) is situated beneath a receiver tank (b) that can be flushed with argon in order to remove oxygen from the dosing unit (valve (d) closed, valves (c) and (e) open). The receiver tank is filled with quartz wool in order to minimize void space with potential accumulation of oxygen. Prior to each gasification experiment, the receiver tank (b) was flushed with argon for at least 10 min. Subsequently, the valves (c) and (e) are closed to prevent oxygen from entering the receiver tank (b) and valve (d) is opened. Argon flows down the conus (f) of the dosing unit and serves as a carrier gas for the char. Eventually, the brass cylinder (a) is turned by 180° and the char falls out of the dosing unit being carried onto a quartz wool bed inside the reactor by the gas flow.

Fig. 3B shows the arrangement inside the single-particle reactor during a gasification experiment. The char sample is placed on a quartz wool bed while the feed gas flows top-down. Beneath the quartz wool bed, a quartz glass tube with fused-in quartz frit is located. In order to measure the temperature of the char sample, a type K thermocouple is inserted via a quartz glass capillary tube that is fused into the frit. The end of the quartz glass tube is sealed with a stuffing box packing (not shown in Fig. 3B), i.e. a ceramic fiber rope that prevents an idle gas flow past the char sample and the quartz glass tube.

Prior to each gasification experiment, the desired reaction temperature was set by means of the type K thermocouple within the quartz glass capillary in the single-particle reactor under constant argon flow and atmospheric pressure using the electric furnace. Reaction temperatures were varied between 810 °C and 870 °C. During gasification stage

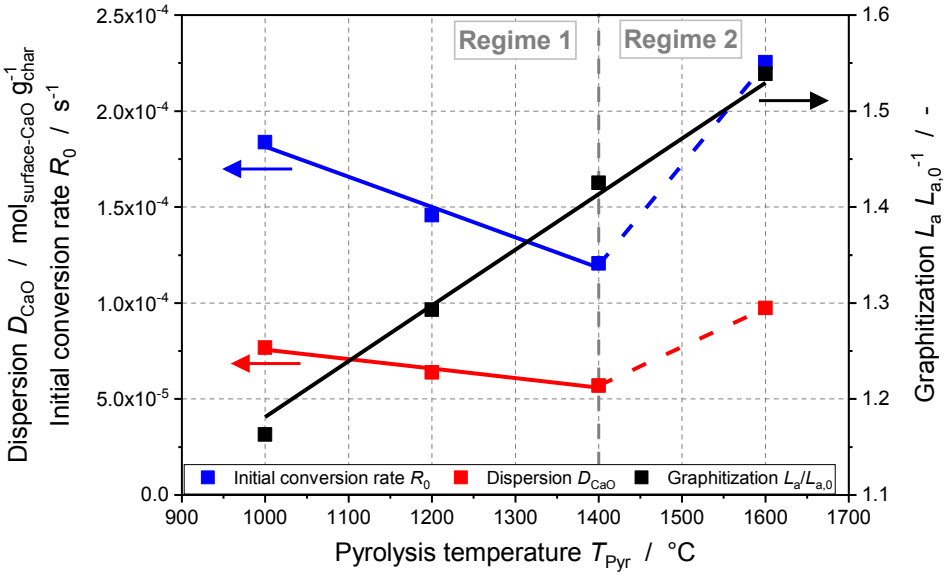

Fig. 1. Summary of the most important experimental results (CaO dispersion D_{CaO}, initial conversion rate R_0 and graphitization degree L_a $L_{a,0}^{-1}$) for the secondary chars pyrolyzed between 1000 °C and 1600 °C [32].

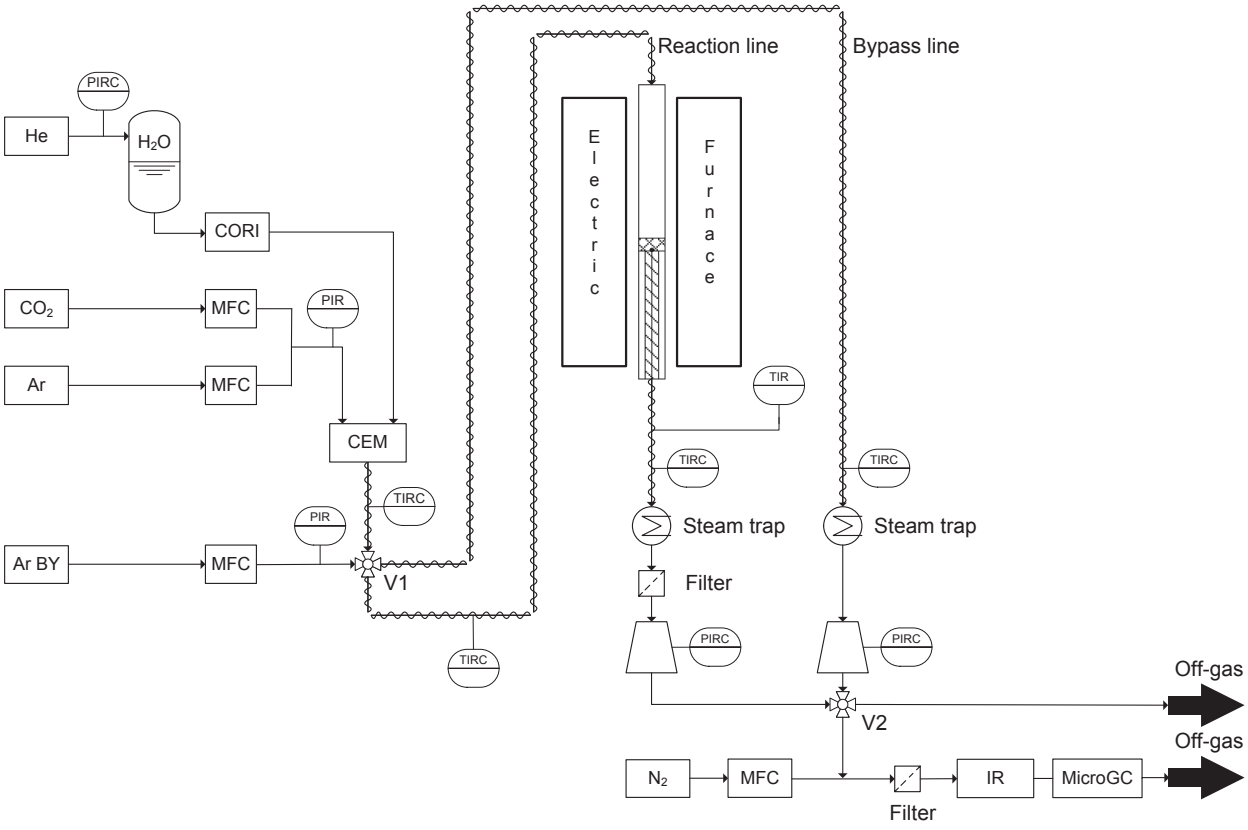

Fig. 2. Schematic flow diagram of the single-particle reactor used for pressurized gasification experiments.

of the experiments, the temperature deviations detected where within ± 1 K. Subsequently, the char sample was filled into the bore of the brass cylinder and the dosing unit was mounted on top of the reactor after being flushed with argon. For the experiments in CO_2 atmosphere, a sample amount of 50 mg was chosen while the experiments in H_2O and mixed CO_2/H_2O atmospheres were carried out using 20 mg. The sample mass was determined in preliminary studies in order to eliminate diffusional effects and ensure the differential operation of the reactor maintaining a concentration deviation of the educts below 3 vol-%. After directing the argon flow through the cone of the dosing unit, the brass

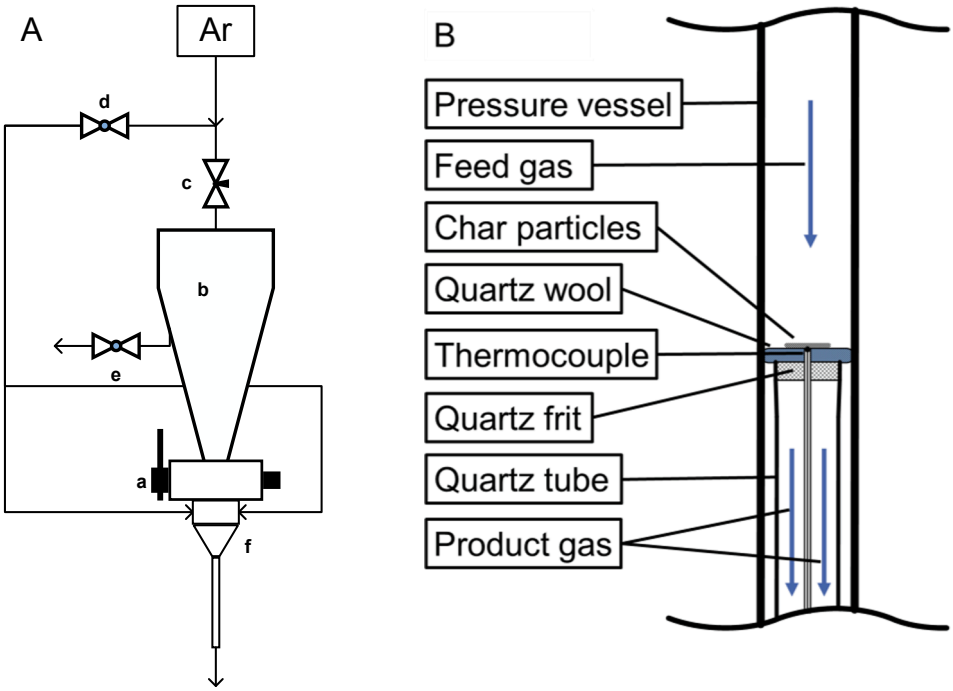

Fig. 3. Schematic illustration of the dosing unit (A) (a, brass cylinder; b receiver tank; c-e, valves; f conus) and the arrangement inside the single-particle reactor (B).

cylinder was turned by 180° and the char sample fell onto the quartz wool bed. Immediately after, a slight increase in the CO concentration was observed via IR in the order of few ppm due to partial combustion of char with oxygen that was still adsorbed on the char surface. After few seconds, the CO signal reached baseline level again. The calculated amount of fixed carbon being combusted in this step was estimated to be approx. 3.2% for P1400 and 0.6% for P1600 accounting for a worst case where the whole micropore surface area is occupied with air (21% oxygen and 79% nitrogen). For the calculation, it was assumed that the edge carbon atoms lie in the (1 0 0) plane and each carbon atom occupies an area of $8.3{\cdot}10^{-20}$ m^2 [40].

At this stage of the experiment, argon flows through both lines (reaction and bypass) with 1 l min^{-1} at atmospheric pressure. Before the gasification started, valve V1 was set to position B, at which the reactant gases are led to the bypass line and argon (Ar BY) flows through the reaction line. Subsequently, the reactant gas composition was adjusted in the bypass line and the desired system pressure was set in both lines using the back pressure regulators. The total volumetric flow rate of the reactant gases was adapted for each experiment in order to maintain a constant superficial linear gas velocity of 21 cm s^{-1} for the CO_2 and 10.5 cm s^{-1} for the H_2O and mixed atmosphere gasification experiments at reaction conditions. These values were determined in preliminary studies and also depend on the chosen sample amounts in order to eliminate diffusional effects and operate the reactor differentially. The reactant gas composition was checked using gas phase analytics (IR and MicroGC) setting valve V2 to position B. Immediately after the gas phase analysis, valve V2 was switched back to position A. To begin the gasification experiment, valve V1 was set to position A as well. The change in product gas concentration was monitored online via IR and the MicroGC took samples every 3 min. All further data evaluation is based on the MicroGC measurements. A gasification experiment was terminated when the measured volume fraction of the product gases was in the range of a low two-digit ppm value and did not change for at least two MicroGC measurements. An overview of all experiments conducted for single atmosphere and mixed gasification process conditions can be found in Tables 4–6.

Table 4
Process conditions during CO_2 gasification of P1400 and P1600.

v_{gas} cm s^{-1}	m_{sample} mg	T °C	p_{tot} bar	p_{CO_2} bar
21	50	830	1	1
		850	5	5
		870	10	10
			15	15
			20	5
				10
				15
				20

Table 5
Process conditions during H_2O gasification of P1400 and P1600.

				P1400	P1600
v_{gas} cm s^{-1}	m_{sample} mg	T °C	p_{tot} bar	p_{H_2O} bar	p_{H_2O} bar
10.5	20	830	1	0.2	0.2
		850		0.4	
		870	2	0.4	0.4
				0.8	0.8
			5	0.8	
				2	2
			10	2	
				5	5

2.3. Determination of carbon conversion X_C

A common definition for carbon conversion X_C can be written as follows:

$$X_C(t) = \frac{m_{C,0} - m_C(t)}{m_{C,0}} \tag{5}$$

$$m_{C,0} = m_{char} x_{C_{fix}} \tag{6}$$

Here, $m_{C,0}$ represents the initial mass of fixed carbon, $m_C(t)$ is the

Table 6
Process conditions during mixed gasification of P1400 and P1600.

v_{gas} cm s^{-1}	m_{sample} mg	T °C	p_{tot} bar	p_{H_2O} bar	p_{CO_2} bar
10.5	20	810	5	0.8	0.8
		830			
		850			
		830	5	0.8	2
				2	0.8
			10	0.8	5
				2	2
			15	2	5
			20	5	5

remaining carbon mass at a certain time t, with m_{char} being the char mass and $x_{C_{fix}}$ being the fixed carbon mass fraction of the char sample. However, the single-particle reactor used in this work does not allow for the measurement of discrete mass signals. In fact, the carbon conversion X_C was determined using a carbon balance and gas phase analysis (see Sections 2.3.1–2.3.3). The carbon mass balance leads to the following differential equation for a fractional carbon conversion dX_C:

$$\frac{dX_C}{dt} = \frac{M_C}{m_{C,gasif}} \dot{n}_{C,out}(t) \tag{7}$$

$\dot{n}_{C,out}(t)$ is the time dependent molar flow rate of carbon containing gasification product gases, M_C the carbon molar mass and $m_{C,gasif}$ the total mass of gasified carbon. The gasification product gases considered for $\dot{n}_{C,out}(t)$ differed for each gasification experiment, i.e. CO_2, H_2O and mixed CO_2/H_2O atmospheres. During CO_2 gasification, only CO was taken into account (see Section 2.3.1) while during H_2O gasification, CO and CO_2 had to be considered due to water–gas shift reaction (see Section 2.3.2). Based on an approach from Chen et al. [17] for mixed CO_2/H_2O gasification, the volume fraction of hydrogen produced was taken into account for $\dot{n}_{C,out}(t)$ during mixed gasification experiments (see Section 2.3.3).

The gasified mass of carbon $m_{C,gasif}$ can be calculated via integration of the molar flow rate of carbon containing gasification product gases $\dot{n}_{C,out}(t)$ from $t = 0$ to the end of the experiment at t_{end} and the carbon molar mass M_C.

$$m_{C,gasif} = M_C \int_0^{t_{end}} \dot{n}_{C,out}(t)dt \tag{8}$$

The molar flow rate $\dot{n}_{out}$ of all permanent gases exiting the reactor and being detected in gas phase analytics was calculated using the nitrogen reference flow $\dot{V}_{N_2}$, the nitrogen volume fraction $y_{N_2}(t)$ and the molar volume $V = 22{,}414$ l mol^{-1}. In the frame of this work, molar and volume fractions were considered to be equal (ideal gas), since gas phase analytics were operated at atmospheric pressure.

$$\dot{n}_{out}(t) = \frac{\dot{V}_{N_2}}{y_{N_2}(t)V} \tag{9}$$

For the subsequent determination of the initial conversion rate R_0 and reaction rate r_i (see Section 2.4), the carbon conversion X_C was always based on the gasified mass of carbon $m_{C,gasif}$ calculated from gas phase data as described above. A comparison of $m_{C,gasif}$ with the value of the initially weighed out carbon mass $m_{C,0}$ was conducted for each experiment allowing for an evaluation of the methodological approach.

2.3.1. Gasification with CO_2

During experiments with CO_2, the only gasification product gas considered for $\dot{n}_{C,out}(t)$ was CO. In this case, the gasified mass of carbon $m_{C,gasif,CO_2}$ is calculated using the CO molar fraction y_{CO} taking into account the stoichiometry of the Boudouard reaction.

$$m_{C,gasif,CO_2} = \frac{M_C}{2} \int_0^{t_{end}} y_{CO}(t)\dot{n}_{out}(t)dt \tag{10}$$

$$X_{C,gasif,CO_2}(t) = \frac{\int_0^t y_{CO}(t)\dot{n}_{out}(t)dt}{\int_0^{t_{end}} y_{CO}(t)\dot{n}_{out}(t)dt} \tag{11}$$

Based on this approach, the carbon conversion X_C always reaches the value 1 at the end of an experiment as the carbon balance is carried out for the gas phase. Comparing the initially weighed out amount of carbon $m_{C,0}$ with $m_{C,gasif,CO_2}$, the carbon mass balance was closed between 78% and 98% for the gasification experiments with CO_2.

2.3.2. Gasification with H_2O

The carbon containing product gases during gasification with H_2O included not only CO but also CO_2. Since CO can be converted to CO_2 via water–gas shift (WGS) reaction in the presence of H_2O, both gases were considered as a measure for the amount of carbon gasified. Due to the low amount of methane (two orders of magnitude lower than the other product gases) found in the product gas, CH_4 was neglected in the carbon balance. The error in carbon balance was estimated to be approx. 0.5%. The mass balance based on the initially weighed out amount of carbon $m_{C,0}$ was closed between 66% and 93% for the gasification experiments with H_2O.

$$m_{C,gasif,H_2O} = M_C \int_0^{t_{end}} (y_{CO}(t) + y_{CO_2})\dot{n}_{out}(t)dt \tag{12}$$

$$X_{C,gasif,H_2O}(t) = \frac{\int_0^t (y_{CO}(t) + y_{CO_2})\dot{n}_{out}(t)dt}{\int_0^{t_{end}} (y_{CO}(t) + y_{CO_2})\dot{n}_{out}(t)dt} \tag{13}$$

2.3.3. Gasification in mixed CO_2/H_2O atmospheres

For the gasification in mixed CO_2/H_2O atmospheres, another approach had to be taken since it is difficult to distinguish between CO_2 from the feed gas and CO_2 formed due to WGS reaction converting CO in the presence of H_2O. According to Chen et al. [17], the following reactions need to be taken into account during mixed gasification (methane formation being neglected).

a $C + CO_2 \rightleftharpoons 2CO$ (R11)

b $C + H_2O \rightleftharpoons H_2 + CO$ (R12)

c $CO + H_2O \rightleftharpoons CO_2 + H_2$ (R13)

Introducing global reaction rates a, b and c (in mol s^{-1}) for (R11)–(R13), the following expressions can be written for the molar flow rates of the gasification product gases involved. The consumption of carbon is considered in Eq. (17).

$$\dot{n}_{CO} = 2a + b - c \tag{14}$$

$$\dot{n}_{H_2} = b + c \tag{15}$$

$$\dot{n}_{CO_2} = -a + c \tag{16}$$

$$-\dot{n}_C = a + b \tag{17}$$

From Eqs. (14), (15) and (17), the carbon consumption $\dot{n}_C$ can be rewritten as the molar flow rate of carbon containing gasification product gases $\dot{n}_{C,out,mix}(t)$ during mixed CO_2/H_2O atmosphere gasification using CO and H_2 molar fractions. The mass balance based on the weighed out amount of carbon $m_{C,0}$ was closed between 57% and 75% for the gasification experiments in mixed CO_2/H_2O atmospheres. A possible source of error for the lower balance closures during H_2O and mixed H_2O/CO_2 gasification is the absorption of CO_2 in the condensing water after the reactor. The CO_2 containing water is extracted from the system in the steam trap that is operated at reaction pressure. Thus, the higher the reaction pressure, the more CO_2 was solved in the water and

removed from the system. This reduces the total molar flow rate $\dot{n}_{out}$ and the CO_2 concentration prior to gas phase analysis and therefore worsens the carbon balance. Another reason is that for balancing purposes, only permanent gases were taken into account. The steam trap is operated at 5 °C. A complete removal of water from the product gas is technically hard to achieve without increasing the delay time of the whole plant dramatically. Thus, the product gas still contains water to a small extent, which corresponds to the dew point concentration at 5 °C. This amount of water was neglected in the carbon balance calculations.

Concerning the gasification in mixed H_2O/CO_2 atmospheres, more Micro GC calibration points for hydrogen in the low ppm area (<5000 ppm) could have further minimized errors and ameliorated the carbon balance.

$$-\dot{n}_C = a + b = \frac{\dot{n}_{CO} + \dot{n}_{H_2}}{2} = \dot{n}_{C,out,mix}(t) = \frac{y_{CO}(t) + y_{H_2}(t)}{2}\dot{n}_{out}(t) \tag{18}$$

$$m_{C,gasif,mix} = M_C \int_0^{t_{end}} \left(\frac{y_{CO}(t) + y_{H_2}(t)}{2}\dot{n}_{out}(t) \right) dt \tag{19}$$

$$X_{C,gasif,mix}(t) = \frac{\int_0^t \left(\frac{y_{CO}(t)+y_{H_2}(t)}{2}\dot{n}_{out}(t) \right) dt}{\int_0^{t_{end}} \left(\frac{y_{CO}(t)+y_{H_2}(t)}{2}\dot{n}_{out}(t) \right) dt} \tag{20}$$

2.4. Determination of reaction rate r_i

Carbon conversion $X_C(t)$ was determined using gas phase analytics and the equations presented in Section 2.3. The conversion rate R_X can be calculated via carbon balance as presented in Eq. (21).

$$R_X = \frac{dX_C}{dt} = \frac{M_C}{m_{C,gasif}}\dot{n}_{C,out}(t) \tag{21}$$

Furthermore, R_X is defined by a rate coefficient $R(T,p)$ and a structural term $F(X)$ [25]:

$$R_X = \frac{dX_C}{dt} = R(T,p)F(X_C) \tag{22}$$

In the frame of this work, the Uniform Conversion Model (UCM) was used to model the conversion process resulting in a structural term of $F(X_C) = 1 - X_C$ [41] and the following expression:

$$R_X = \frac{dX_C}{dt} = R_0(1 - X_C) \tag{23}$$

$$R_0 = \left.\frac{dX_C}{dt}\right|_{X_C=0} \tag{24}$$

$$X_C(t) = 1 - \exp(-R_0 t) \tag{25}$$

R_0 is defined as the initial conversion rate, which was determined by a least-square fit in the carbon conversion range between 20% and 50% (see Fig. 4). In the frame of this work, the focus was to determine the initial conversion rate R_0 by fitting the carbon conversion curve between 20% and 50% using the idealized particle conversion model UCM. The UCM treats the fuel particle as a homogeneous body where the gasification reaction occurs uniformly. However, reactivity of the char might highly change in the course of the reaction due to changes in morphology, ash dispersion and graphitization throughout carbon conversion. Therefore, it was decided to use an early stage of gasification for the determination of a characteristic value of R_0 in order to be able to interpret the results based on the char properties analyzed prior to gasification. The carbon conversion range between 20% and 50% was chosen in order to minimize the effects of gas switch at the start of each experiment. Furthermore, the char properties for higher conversion degrees may have changed and were not characterized. Every gasification experiment was repeated two to three times.

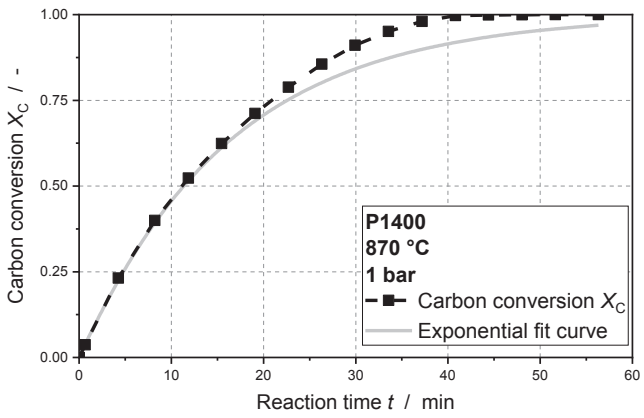

Fig. 4. Carbon conversion X_C and exponential fit curve for the determination of the initial conversion rate R_0 during gasification of P1400 with CO_2 at 870 °C and 1 bar in the single-particle reactor.

Eventually, the reaction rate r_i ($i = CO_2, H_2O$, mix) is calculated using the initial conversion rate R_0 and the molar mass of carbon M_C. All further reaction kinetic parameters were calculated using the experimentally determined reaction rates r_i.

$$r_i = \frac{R_0}{M_C} \tag{26}$$

3. Results and discussion

3.1. Gasification experiments with CO_2

3.1.1. Raw data evaluation

Fig. 5 shows the CO volume fractions y_{CO} and carbon conversion curves $X_{C,gasif,CO_2}$ during gasification of P1400 and P1600 with CO_2 at 830 °C and a total pressure of 1 bar. Carbon conversion $X_{C,gasif,CO_2}$ was calculated using Eq. (11). Both char samples show decreasing CO signals, however, P1600 starts with a higher volume fraction of approx. 0.8 vol-% and decreases faster than the sample P1400. Therefore, the atmospheric gasification experiment with P1600 at 830 °C is already terminated after 100 min whereas the gasification of P1400 lasts approx. 20 min longer. The high starting value and steep decrease of y_{CO} for P1600 leads to a faster increase of carbon conversion $X_{C,gasif,CO_2}$ and thus, to a higher initial conversion rate R_0. Furthermore, the decreasing course of y_{CO}, which was especially pronounced during gasification of P1600, is an indication for Ca catalyzed gasification reaction. Another indication for Ca catalysis during CO_2 gasification may be a decreasing course of conversion rate R_X which is directly correlated with the CO volume fraction y_{CO} as presented in Eqs. (10) and (21). Struis et al. [42] investigated the catalytic activity of different metal elements (Na, K, Ca, Mg, Zn, Pb, Cu) found in waste wood ashes. They observed a high catalytic activity of alkaline earth nitrate salts during the early gasification stage followed by decreasing reaction rate for the whole carbon conversion range. The authors presumed that this decrease arises from sintering of the resulting alkaline earth metal oxides lowering their dispersion on the char surface. Another correlation between char-CO_2 reactivity and CaO dispersion was found by Cazorla-Amoros et al. [43]. The authors investigated the dispersion and sintering of Ca species on carbon samples during pyrolysis and gasification with CO_2. Their results indicated that Ca dispersion decreased with increasing carbon conversion during gasification with CO_2 suggesting a deactivation mechanism presumably due to sintering processes. As expected from the results of our previous work [32], the higher initial conversion rate R_0 of P1600

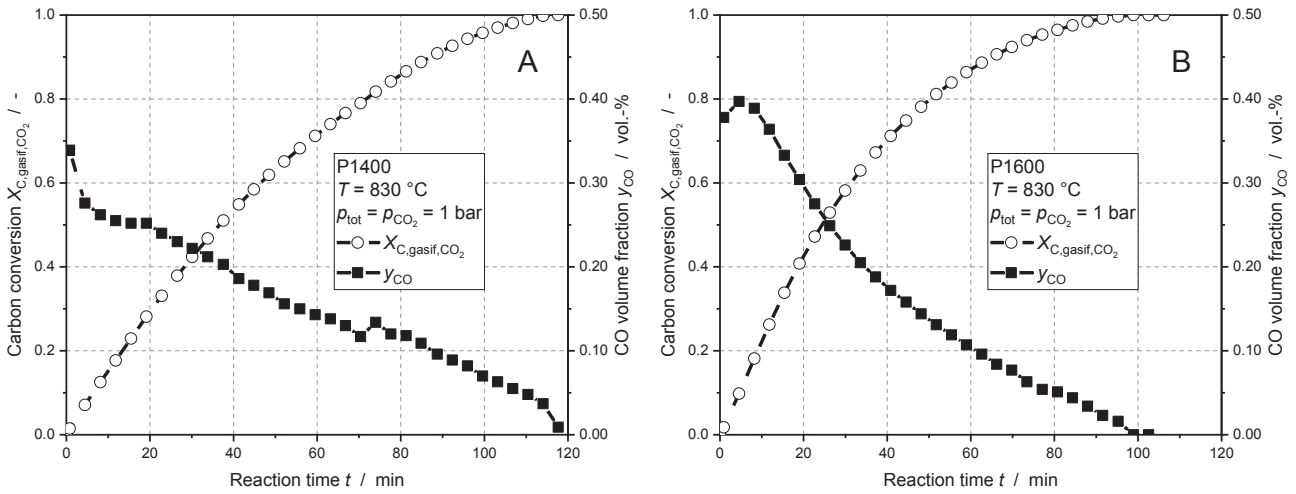

Fig. 5. CO volume fraction y_{CO} and carbon conversion $X_{C,gasif,CO_2}$ during gasification of P1400 (A) and P1600 (B) in CO_2 at 830 °C and 1 bar total pressure.

during gasification with CO_2 was observed for all CO_2 partial pressures and temperatures investigated due to the formation of a thin CaO layer catalyzing the gasification reaction (also see Figs. 7 and 8).

For $p_{CO_2} = 20$ bar, however, both chars showed similar reaction rates (see Fig. 8). Here, the total gasification time of both chars was similar and amounted to approx. 60 min (see Fig. 6). Furthermore, CO volume fractions y_{CO} were in the range of 0.02 for P1400 and 0.03 for P1600, respectively. In comparison to the experiments at lower pressure, a CO volume fraction plateau was obtained for the first 20 min of gasification. This plateau also effects the shape of the carbon conversion curve X_C becoming more linear and may be interpreted as some sort of saturation of the char surface for this CO_2 partial pressure and the corresponding char.

3.1.2. *Influence of temperature*

Arrhenius plots for the gasification of P1400 and P1600 with CO_2 partial pressures between 1 bar and 20 bar and temperatures between 830 °C and 870 °C are depicted in Fig. 7. For P1400, an increase of temperature and CO_2 partial pressure leads to an increase in reaction rate. The slope of the lines for a constant partial pressure are almost parallel suggesting no diffusion limitations during the kinetic measurements. Furthermore, the mean activation energy of the P1400 gasification experiments with CO_2 was 310.8 kJ mol^{-1} being rather at the upper limit of the activation energies presented in literature for biogenic char-CO_2 gasification [25]. The high values for the activation energies obtained may also be an indication for the absence of diffusional effects, i.e. the determination of true microkinetics. For P1600, small differences in the Arrhenius plot can be observed compared to P1400. The mean activation energy of the P1600 gasification experiments with CO_2 was slightly lower and accounted for 301.1 kJ mol^{-1}. The large difference in reaction rate r_{CO_2} between the 1 bar and the 5 bar experiments becomes apparent. During gasification of P1600, a slight increase of p_{CO_2} in the low pressure area induces a high increase in char-CO_2 reaction rate. Furthermore, a saturation for the high pressure area can be observed. An increase of p_{CO_2} from 10 bar to 15 bar only marginally increases the reaction rate. Additionally, the increase of p_{CO_2} from 15 bar to 20 bar does not lead to a further increase in reaction rate. It can be assumed that a saturation of the char surface is achieved starting at $p_{CO_2} = 15$ bar for the sample P1600. The lower specific surface area (micropores) of P1600 with 126.4 m^2 g^{-1} in comparison to the sample P1400 with 660.0 m^2 g^{-1} may be a reason for the saturation of the char surface at higher CO_2 partial pressures.

Fig. 8 shows an Arrhenius plot of P1400 and P1600 for 1 bar, 10 bar and 20 bar CO_2 partial pressure to facilitate a direct comparison between both char samples. Once again, it is remarkable that the reactions rates r_{CO_2} of P1600 are higher than the rates of P1400 for one constant pressure despite the higher graphitization degree and the lower micropore surface area of P1600. Higher char-CO_2 reaction rates of P1600 compared to P1400 were determined for all reaction conditions investigated. At the highest pressure of 20 bar, however, both chars showed

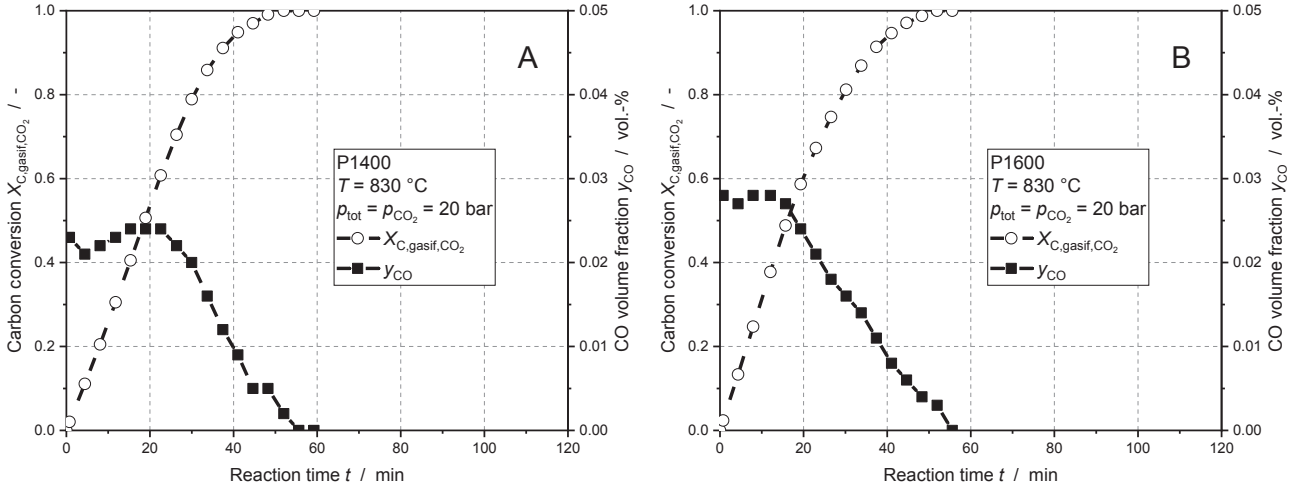

Fig. 6. CO volume fraction y_{CO} and carbon conversion $X_{C,gasif,CO_2}$ during gasification of P1400 (A) and P1600 (B) in CO_2 at 830 °C and 20 bar total pressure.

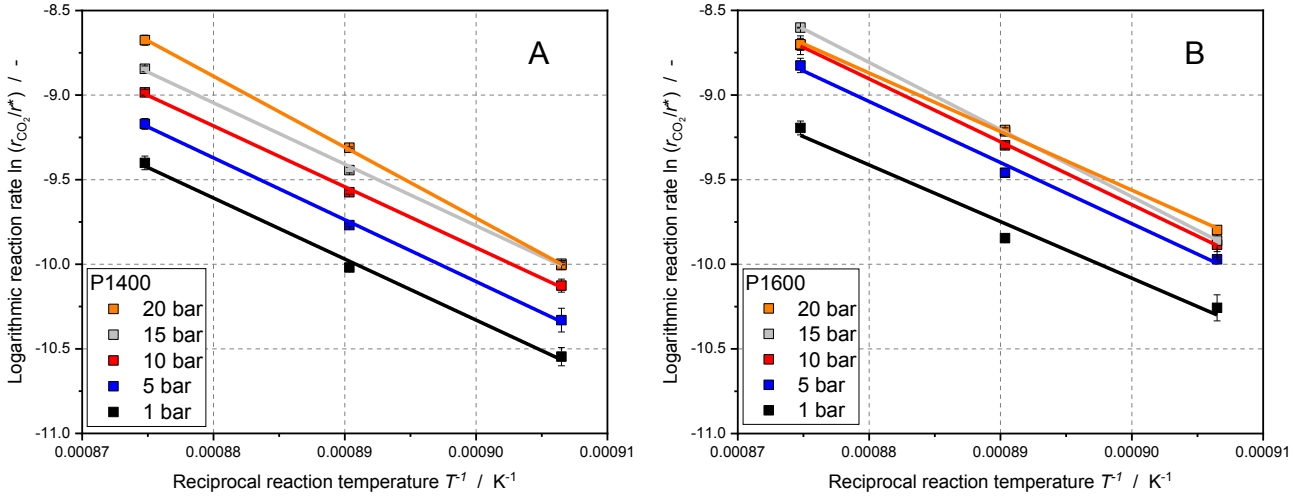

Fig. 7. Arrhenius plots for the gasification of P1400 (A) and P1600 (B) in CO_2 (p_{CO_2} = 1–20 bar and T = 830–870 °C).

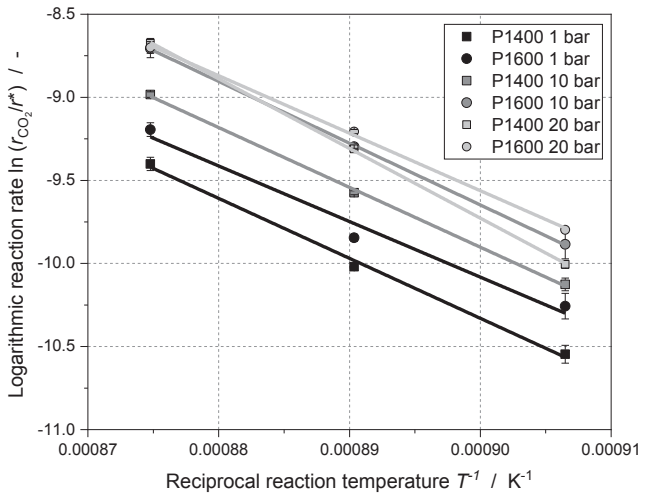

Fig. 8. Arrhenius plot for the gasification of P1400 and P1600 in CO_2 (p_{CO_2} = 1 bar, 10 bar, 20 bar and T = 830–870 °C).

similar reaction rates towards CO_2.

3.1.3. *Influence of total pressure and CO_2 partial pressure*

In Fig. 9, the char-CO_2 reaction rates are depicted as a function of CO_2 partial pressure. Experiments were conducted either with varying total pressure ($p_{tot} = p_{CO_2}$, dark symbols) or with constant total pressure of 20 bar for varying CO_2 partial pressures between 5 bar and 15 bar (open symbols). Results indicate that the influence of total pressure may be negligible as the experiments with a constant total pressure are mostly within the standard deviation of the experiments where CO_2 partial pressure equals total pressure. Slight differences between both experimental approaches may have arisen from the rather high dilution of product gases at a total pressure of 20 bar. Thus, the important parameter was considered to be CO_2 partial pressure or CO_2 concentration, respectively. Therefore, only the experiments where CO_2 partial pressure equals total pressure were taken for modeling purposes (see Section 3.1.4). Concerning the comparison between both chars, following observations can be made: CO_2 reaction rate r_{CO_2} of P1400 increases almost linearly with increasing CO_2 partial pressure showing no signs of saturation at high pressures. On the contrary, the CO_2 reaction rate of P1600 increases strongly between 1 bar and 5 bar and forms a plateau at higher pressures as could also be seen in the Arrhenius plot (see Fig. 7).

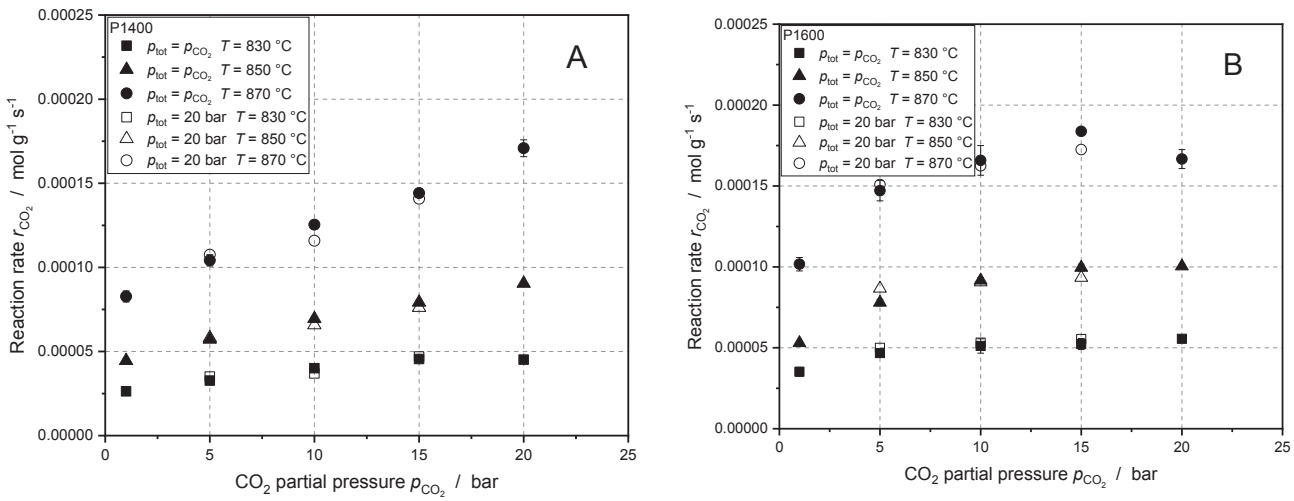

Fig. 9. Influence of total and CO_2 partial pressure on reaction rate r_{CO_2} during gasification of P1400 (A) and P1600 (B) (T = 830–870 °C, diluting gas: argon).

3.1.4. Reaction kinetic modeling

Power law. Fig. 10 shows the experimentally determined reaction rates r_{CO_2} of P1400 and P1600 modeled with a power law approach (see Eq. (2)). The corresponding model parameters k_{0,CO_2}, E_{A,CO_2} and n_{CO_2} can be taken from Table 7. Results indicate that basically, power law is a suitable approach for modeling pressurized char-CO_2 gasification of both samples. However, the specific characteristics of each char that are induced by its pre-gasification history and origin are rather poorly represented i.e. the linear increase of r_{CO_2} with increasing CO_2 partial pressure during gasification of P1400 cannot be adequately described using a power law approach. In addition, the reaction rates at 20 bar are rather underestimated. Concerning the sample P1600, a saturation at CO_2 partial pressures of 10 bar and above was determined. Again, the power law approach is not able to describe this phenomenon for very high pressures and overestimates the values at $p_{CO_2} = 20$ bar. All experimental values determined during pressurized gasification of P1400 and P1600 with CO_2 can be modeled within a deviation of ± 20% using the power law approach.

In order to compare the kinetic parameters determined in this work with similar studies, a discussion based on the values reported in literature is conducted for CO_2 and H_2O gasification, respectively. Fermoso et al. [44] investigated the gasification reaction of pine wood chars with CO_2 that were pyrolyzed in a drop tube reactor at 1000 °C and 1400 °C. The gasification experiments were conducted in a TGA at elevated pressure. During high-pressure experiments, the activation energies obtained (144 kJ mol^{-1}–164 kJ mol^{-1}) were rather low as compared to the activation energies determined at atmospheric pressure (184 kJ mol^{-1}–246 kJ mol^{-1}). This might be an indication for artefacts (e.g. diffusional limitations) evoked by the experimental methodology due to a limited gas flow (75 cm^3 min^{-1}) in the TGA resulting in a low gas velocity during high-pressure experiments. Besides, several particle conversion models were used i.e. the volumetric model, the grain model and the random pore model. No significant differences in the calculated activation energies were observed using these three models.

Another work was published by Cetin et al. [45] concerning pyrolysis and gasification of different biomass types (pine, eucalyptus and bagasse). Pyrolysis was carried out at 950 °C in a wire-mesh reactor at high heating rates (500 K s^{-1}) while pressurized gasification experiments were conducted in a TGA. Their results indicate that the kinetic parameters obtained are strongly dependent on the biomass type investigated. The determined activation energies range between 198 kJ mol^{-1} for bagasse chars and 238 kJ mol^{-1} for pine wood chars.

Gasification experiments with CO_2 in a fixed-bed reactor using different coal chars have been carried out by Li et al. [46]. The coals (lignite, sub-bituminous coal, anthracite) were pyrolyzed at 900 °C for 30 min prior to gasification. The shrinking core model was used to describe the particle conversion during gasification while relatively low activation energies ranging between 120 kJ mol^{-1} and 209 kJ mol^{-1} were obtained. Furthermore, the reaction orders n during CO_2 gasification (0.264–0.312) were similar to the ones presented in this work. The authors were able to show an effect of coal rank on the activation energies determined: the higher the coal rank of the chars, the higher the activation energy obtained. This effect might be caused due to higher degrees of graphitization for increasing coal ranks. Since the beech wood chars investigated in the frame of this work also exhibit a high degree of graphitization (see Section 2.1) due to pyrolysis at very high temperatures, this might be an explanation for the relatively high activation obtained during CO_2 gasification.

Table 7
Kinetic parameters for gasification of P1400 and P1600 with CO_2 using power law approach.

		P1400	P1600
k_{0,CO_2}	mol (g s bar^n)$^{-1}$	1.0163·10^{10}	5.675·10^9
E_{A,CO_2}	kJ mol^{-1}	308.7	300.7
n_{CO_2}	–	0.214	0.186

Atmospheric gasification experiments with chars originating from beech wood were conducted by Guizani et al. [23]. Reaction kinetic parameters were obtained during gasification of beech wood chars that were pyrolyzed at 850 °C–950 °C with a heating rate of approx. 100 K s^{-1}. The pyrolysis step was carried out *in-situ* in a TGA directly before initiating the gasification process. The authors used the char reactivity at a carbon conversion degree of 50% for their kinetic modeling approach. The activation energy was determined to be 154 kJ mol^{-1} being relatively low as compared to the present work. However, this discrepancy may be again explained by differences in the char properties i.e. different graphitization degree due to varying pyrolysis conditions.

Langmuir-Hinshelwood. Fig. 11 shows the CO_2 reaction rates r_{CO_2} of P1400 and P1600 modeled with an LH approach (see Eq. (1)). Model parameters $k_{0,1}$, $k_{0,3}$, $E_{A,1}$ and $E_{A,3}$ can be taken from Table 8. The linear increase of r_{CO_2} with increasing CO_2 partial pressure during gasification of P1400 is even poorer described with the LH approach than with power law. The low pressure area up to 10 bar is overestimated while the high pressure values are underestimated. In terms of parity plot, one point was out of the 20% interval and 4 points were close to the 20% deviation. On the other hand, the saturation of P1600 for high CO_2

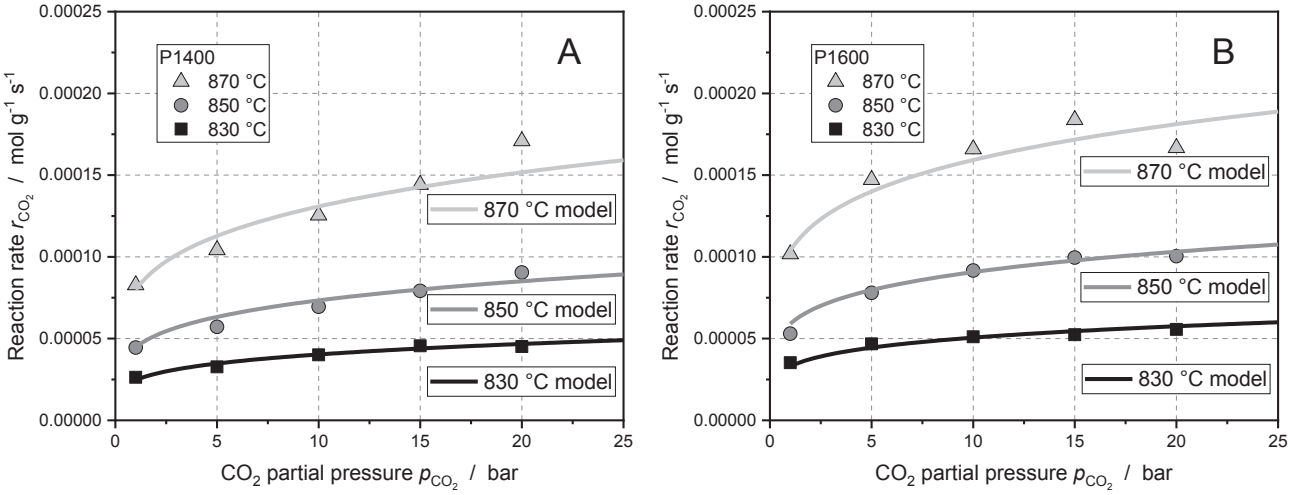

Fig. 10. Modeling of the gasification reaction with CO_2 for P1400 (A) and P1600 (B) using power law approach.

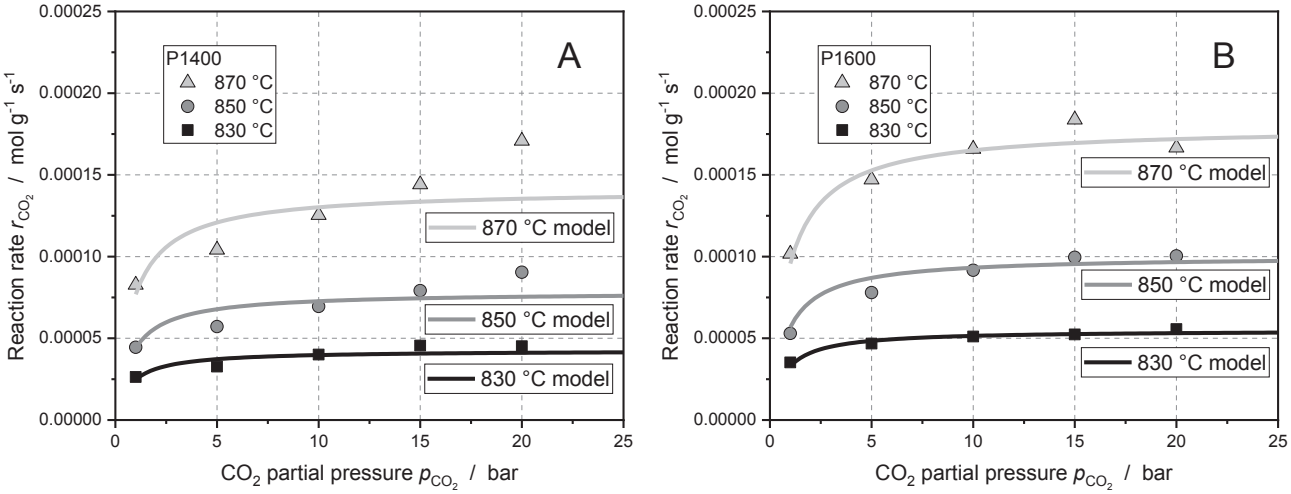

Fig. 11. Modeling of the gasification reaction with CO_2 for P1400 (A) and P1600 (B) using an LH approach.

Table 8
Kinetic parameters for the gasification of P1400 and P1600 with CO_2 using LH approach.

		P1400	P1600
$k_{0,1}$	mol (g s bar)$^{-1}$	$6.80 \cdot 10^{8}$	$2.1 \cdot 10^{7}$
$k_{0,3}$	mol (g s)$^{-1}$	$3.0348 \cdot 10^{10}$	$2.6775 \cdot 10^{10}$
$E_{A,1}$	kJ mol^{-1}	275.9	241.0
$E_{A,3}$	kJ mol^{-1}	313.7	310.2

partial pressures can be modeled precisely using LH approach. Almost all values for P1600 lie within 10% parity. The LH approach describes pressurized gasification of P1600 with CO_2 to full satisfaction.

In summary, it can be stated that the power law approach is suitable to describe gasification kinetics of both chars with CO_2 up to a total pressure of 20 bar. However, the saturation during gasification of P1600 applying high pressures ($p_{CO_2} > 10$ bar) cannot be modeled adequately. Here, the LH approach gives good results, whereas the linear increase of r_{CO_2} with increasing CO_2 partial pressure during gasification of P1400 is described very poorly using the LH approach.

3.2. Gasification experiments with H_2O

3.2.1. Raw data evaluation

Fig. 12 shows the CO and CO_2 volume fractions and carbon conversion curves during gasification of P1400 and P1600 at 830 °C in a mixture of H_2O and Ar. The total pressure was 2 bar while the partial pressure of H_2O was 0.4 bar (rest Ar). The carbon conversion $X_{C,gasif,H_2O}$ is calculated using Eq. (13). In general, H_2O gasification reaction was much faster compared to CO_2 gasification, as can also be seen in literature [25]. Even at H_2O partial pressures of only 0.4 bar and a gasification temperature of 830 °C, carbon conversion $X_{C,gasif,H_2O}$ reached approx. 0.8 within the first 60 min for both char samples. Furthermore, the course of product gas concentrations was rather constant up to a carbon conversion of 0.8 leading to a more linear conversion curve compared to gasification with CO_2. During H_2O gasification of P1400, CO_2 and CO volume fractions were similar at the beginning of the experiment. Both gas concentrations were diverging from each other up to 40 min gasification time. Here, namely at approx. 0.7 carbon conversion, an increase of y_{CO_2} was observed and followed by a steep decrease in both y_{CO} and y_{CO_2}. This decrease was always encountered during gasification with H_2O at a certain carbon conversion degree (mostly between 0.7 and 0.8) depending on the sample and the process conditions applied. The gasification process with H_2O should be considered as finished at this stage of the experiment. The course of the

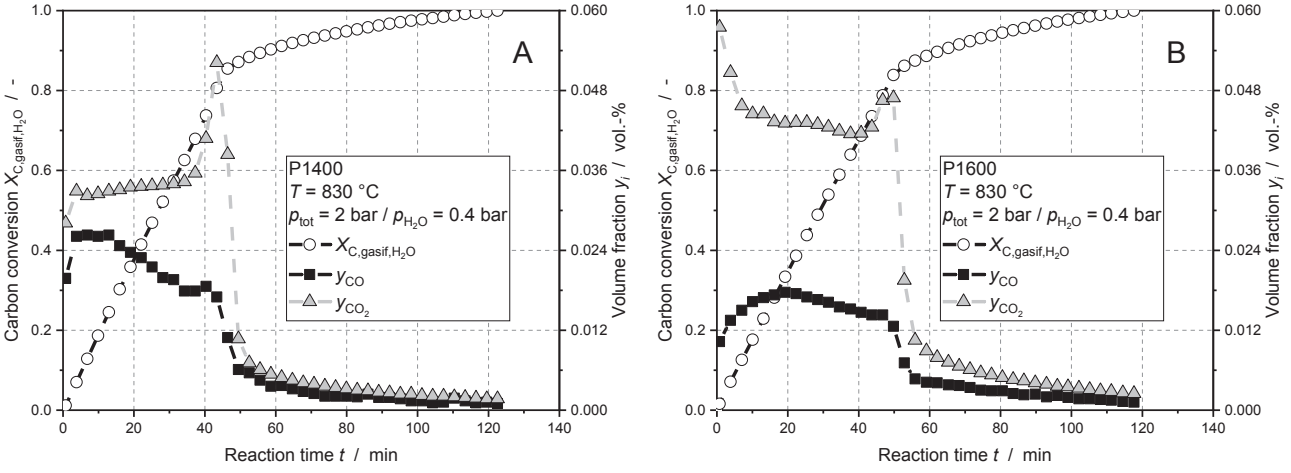

Fig. 12. CO volume fraction y_{CO}, CO_2 volume fraction y_{CO_2} and carbon conversion $X_{C,gasif,H_2O}$ during gasification of P1400 (A) and P1600 (B) with H_2O at 830 °C ($p_{H_2O} = 0.4$ bar, $p_{tot} = 2$ bar, diluting gas: argon).

product gas concentration may be caused by fragmentation of the char particles and back-mixing effects in the exhaust-gas line of the experimental set-up. Since H_2O gasification was much faster than CO_2, the volume fractions of the product gases decreased erratically from a higher level compared to CO_2 gasification where a steady decrease of CO concentration was observed. However, for the determination of initial conversion rates R_0, the experimental and methodological approach should deliver reasonable and reliable data.

Concerning gasification of P1600, again, at around 0.8 carbon conversion, a steep decrease in product gas concentration was observed suggesting that gasification was mainly terminated. Furthermore, CO_2 volume fraction was approx. 4 times the value of y_{CO}. Therefore, it was essential to consider all carbon containing product gases in order to determine a valid initial conversion rate R_0 because of possible changes in product gas concentration due to water–gas shift equilibrium. The existing set-up did not allow to measure the temperature profile of the lower part of the reactor. Therefore, slight differences in product gas concentration could occur because gas temperature at the exit of the reactor may have varied. For future experiments, the simple type K thermocouple recording char temperature will be substituted by a multipoint thermocouple that allows for the recording of a temperature profile in the lower part of the reactor including gas exit temperature.

3.2.2. Influence of temperature

Fig. 13 shows Arrhenius plots for the gasification of P1400 and P1600 with H_2O partial pressures between 0.2 bar and 5 bar and temperatures between 830 °C and 870 °C. Argon was used as carrier gas and H_2O volume fraction was set between 0.2 and 0.5 in the feed gas·H_2O Arrhenius plots can be subsumed since similar trends were observed for both char samples. As for gasification with CO_2, reactions rates r_{H_2O} increase with increasing temperature and reactant gas partial pressure. From the Arrhenius plots, no saturation at the highest pressures investigated can be deduced. The mean activation energy of the P1400 gasification experiments with H_2O was 263.6 kJ mol^{-1} being lower than activation energies for biogenic char-CO_2 gasification which is consistent with literature data [25]. The mean activation energy of the P1600 gasification experiments was slightly lower compared to P1400 and amounted to 234.8 kJ mol^{-1}. Both values for E_{A,H_2O} are also situated in the upper range of activation energies for biogenic char-H_2O gasification reported in literature [25]. Again, this may be an indication for the absence of diffusional effects and the determination of true microkinetics.

Fig. 14 shows an Arrhenius plot of P1400 and P1600 for H_2O partial pressures of 0.2 bar, 0.8 bar and 5 bar to facilitate the direct comparison between both char samples. It becomes apparent that P1400 shows

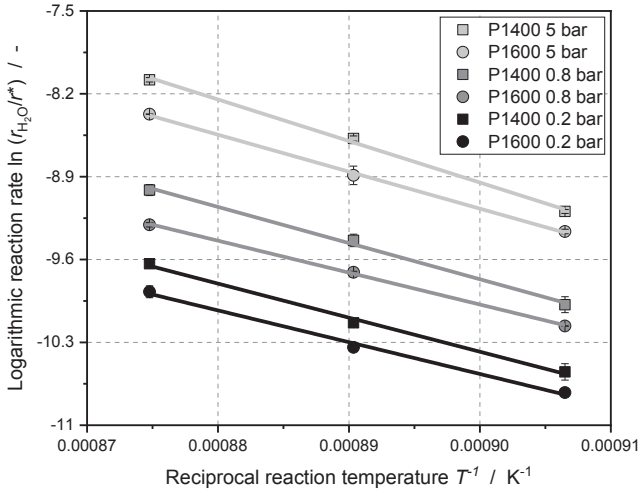

Fig. 14. Arrhenius plot for the gasification of P1400 and P1600 with H_2O (p_{H_2O} = 0.2 bar, 0.8 bar, 5 bar and T = 830–870 °C, diluting gas: argon).

higher reactivity towards H_2O than P1600 which is contrary to the results of CO_2 gasification. However, this finding is what would normally be expected from literature taking into account the higher pyrolysis temperatures of P1600 inducing thermal deactivation due to higher degrees of graphitization and lower micropore surface area. Therefore, it can be stated that the catalytically active CaO film being responsible for the higher initial conversion rates R_0 of P1600 during gasification with CO_2 is of minor significance when gasification is carried out with H_2O. Thus, the dominating char properties affecting H_2O reactivity were considered to be constitution of carbon matrix (i.e. graphitization degree) and micropore surface area.

3.2.3. Influence of total pressure and H_2O partial pressure

Fig. 15 shows an Arrhenius plot illustrating the influence of total pressure during H_2O gasification experiments. Gasification was conducted with P1400 using three different H_2O partial pressures (0.4 bar, 0.8 bar and 2 bar) and varying total pressures (1 bar, 2 bar, 5 bar and 10 bar). Results indicate that very similar reaction rates and activation energies were obtained using two different total pressures. Experiments with p_{H_2O} = 0.8 bar and total pressures of 2 bar and 5 bar, respectively deviated slightly more from each other. Generally, two reasons for possible deviations using different total pressures were identified. First, errors may arise due to higher dilution of product gases at high pressures. Since superficial linear gas velocity was constant during

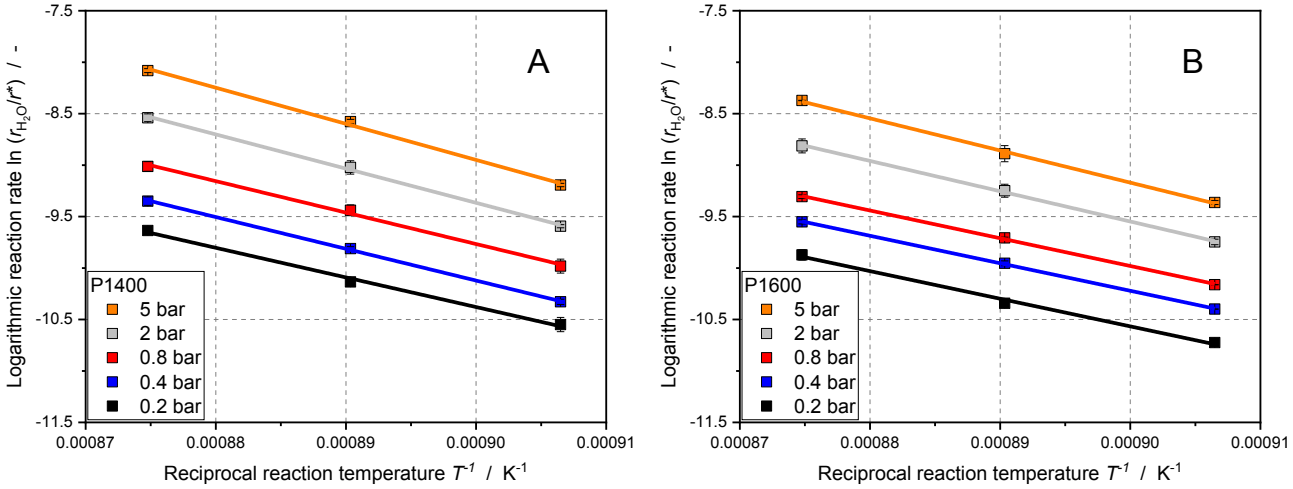

Fig. 13. Arrhenius plots for the gasification of P1400 (A) and P1600 (B) with H_2O (p_{H_2O} = 0.2–5 bar, y_{H_2O}= 0.2–0.5 and T = 830–870 °C, diluting gas: argon).

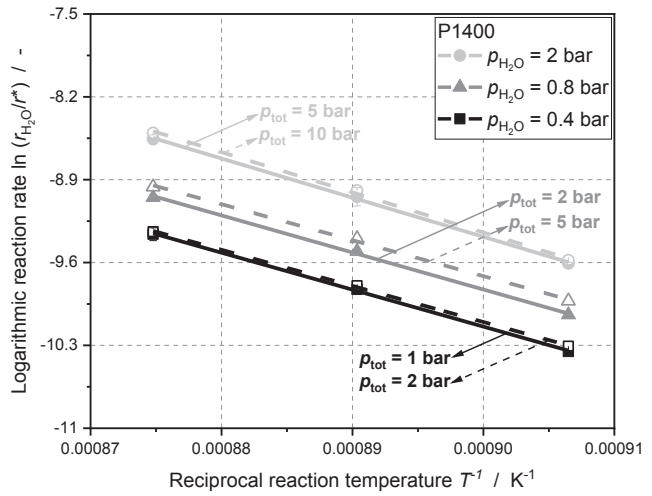

Fig. 15. Influence of total pressure on reaction rate r_{H_2O} during gasification of P1400 with H_2O (T = 830–870 °C, diluting gas: argon).

experiments, volumetric flow rates increased with increasing total pressure. Therefore, product gas concentrations were lower and more difficult to detect using the MicroGC during high pressure experiments. Another possible cause for deviations in the reaction rate determined may originate from absorption of product gases in the condensing water of the steam trap. The three most abundant product gases identified during H_2O gasification were H_2, CO and CO_2. H_2 and CO have relatively low solubility in water compared to CO_2 and may be negligible [47]. Furthermore, CO_2 volume fractions were found to be higher than CO in the exhaust gas suggesting that water–gas shift reaction took place to a certain extent. Increasing the total pressure would lead to significant absorption of CO_2 in water [48] resulting in removal of carbon from the system worsening carbon balance closure. Both phenomena would lead to a shorter reaction time und thus, higher reaction rates applying higher total pressures which is exactly what can be seen in Fig. 15. Consequently, reaction kinetic measurements with H_2O were conducted using rather low total pressures while keeping H_2O volume fractions y_{H_2O} between 0.4 and 0.5 during the experiments above atmospheric pressure.

Fig. 16 shows the reaction rates r_{H_2O} of P1400 and P1600 as a function of H_2O partial pressure. It can be concluded that P1400 exhibits higher reaction rates for all process conditions investigated during H_2O gasification presumably due to lower specific surface area and higher graphitization degree of P1600. Furthermore, no saturation at higher pressures was observed for both chars and the course of experimental data can be well described using a root function. Reaction kinetic modeling of H_2O gasification is presented in Section 3.2.4.

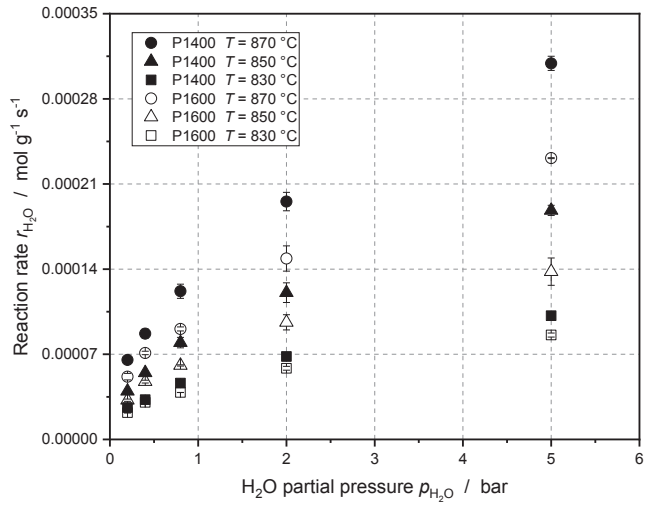

Fig. 16. Influence of H_2O partial pressure on reaction rate r_{H_2O} during gasification of P1400 and P1600 (T = 830–870 °C, diluting gas: argon).

3.2.4. Reaction kinetic modeling

Power law. Fig. 17 shows the experimentally determined reaction rates r_{H_2O} of P1400 and P1600 modeled with a power law approach (see Eq. (4)). The corresponding model parameters k_{0,H_2O}, E_{A,H_2O} and n_{H_2O} can be taken from Table 9. Results indicate that power law is a very suitable method for modeling pressurized char-H_2O gasification of both samples within the process conditions presented in this work. The quality of the power law model was again tested in a parity plot giving a very high goodness of fit. All experimental values determined during pressurized gasification of P1400 and P1600 with H_2O were at least within a deviation of ± 10% using the power law approach.

LH approach does not give good modeling results for both chars since saturation effects were not detected under the process conditions applied. Therefore, LH diagrams and the corresponding model parameters are not shown here but can be found in the supplementary data section.

Again, a comparison with kinetic parameters found in literature is conducted. Li et al. [46] investigated different coals (lignite, subbituminous coal, anthracite) in terms of reactivity towards CO_2 and H_2O in a fixed-bed reactor (cf. Section 3.1.4). For gasification with H_2O, the activation energies obtained with the shrinking core model were relatively low ranging between 114 kJ mol^{-1} and 138 kJ mol^{-1} as compared to the present work. The trend observed during CO_2 gasification concerning higher activation energies for higher rank coals is still valid for H_2O gasification. Furthermore, the reaction orders n during H_2O gasification (0.428–0.493) were similar to the ones presented in this work. The effect of coal rank on activation energy during gasification of different coal chars with H_2O in a fixed-bed reactor was also observed by Yan et al. [49].

Guizani et al. [23] obtained a relatively low activation energy of 139 kJ mol^{-1} during atmospheric gasification of beech wood char with H_2O (cf. Section 3.1.4) as compared to the present work. Again, the rather mild pyrolysis conditions may be an explanation for this discrepancy.

Roberts & Harris [50] and Matsuoka et al. [51] investigated the pressurized gasification reaction of various coal chars with H_2O and obtained activation energies in the range of 221 kJ mol^{-1} to 235 kJ mol^{-1} and 250 kJ mol^{-1}, respectively, both using the uniform conversion model. These activation energies are very similar to the ones presented in this work. Roberts & Harris [50] produced coal chars at 1100 °C with a residence time of 3 h and a low heating rate of 10 K min^{-1} and conducted the subsequent gasification experiments in a pressurized TGA. Matsuoka et al. [51] generated coal chars at 900 °C in a bubbling fluidized bed reactor where the gasification experiments with H_2O were conducted as well.

3.3. Gasification experiments in mixed H_2O/CO_2 atmospheres

3.3.1. Raw data evaluation

Fig. 18 shows the CO and H_2 volume fractions and carbon conversion curves during gasification of P1400 and P1600 at 830 °C in a mixture of CO_2, H_2O and argon. Total pressure was 5 bar while partial pressures of CO_2 and H_2O were 0.8 bar, respectively (rest argon). The carbon conversion $X_{C,gasif,mix}$ was calculated using Eq. (20). The main characteristics of the product gas concentrations during mixed gasification appear to be a superposition of both single atmosphere gasification experiments. First, H_2 and CO volume fractions decrease steadily up to carbon conversion degrees of approx. 0.8. Especially, the decrease of the product

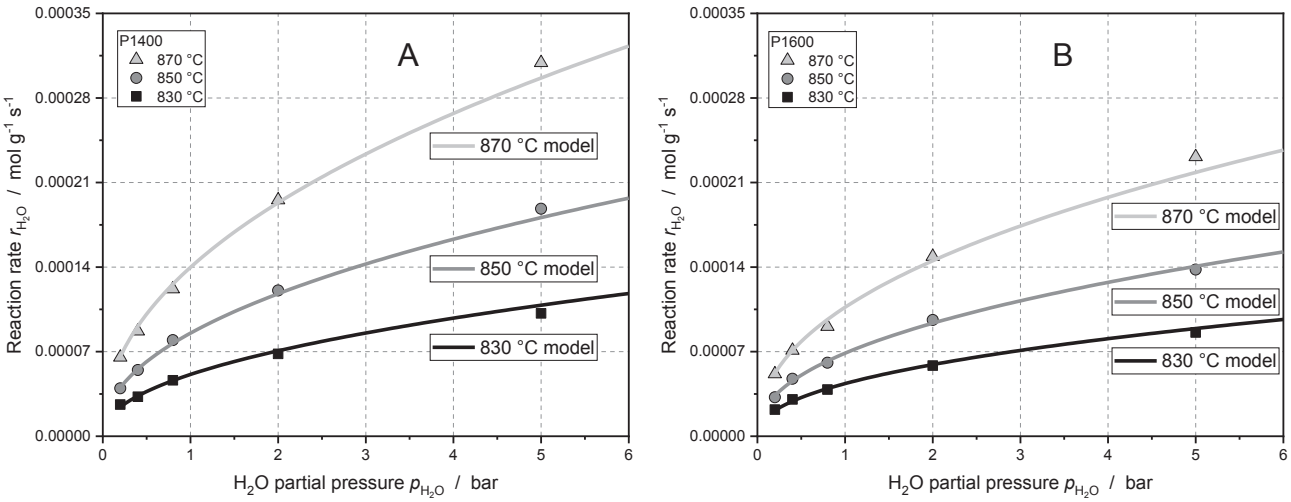

Fig. 17. Modeling of the gasification reaction with H_2O for P1400 (A) and P1600 (B) using power law approach.

Table 9
Reaction kinetic parameters for gasification of P1400 and P1600 with H_2O using power law approach.

		P1400	P1600
k_{0,H_2O}	mol (g s bar^n)$^{-1}$	$1.55 \cdot 10^8$	$5.7 \cdot 10^6$
E_{A,H_2O}	kJ mol^{-1}	263.6	234.8
n_{H_2O}	–	0.467	0.445

gas concentration during P1600 gasification with a steep slope reminds of the course of CO during single CO_2 gasification (see Fig. 5). This may be an indication that Ca catalysis is again dominating CO_2 gasification during mixed experiments [42,43]. The steady decrease in product gas concentration up to $X_{C,gasif,mix} = 0.8$ also leads to a less linear and more exponential shape of the carbon conversion curve of P1600. Second, the strong decrease at $X_{C,gasif,mix} = 0.8$ conversion degree is a characteristic of H_2O gasification experiments and may be caused by particle fragmentation and/or back-mixing effects in the experimental set-up.

3.3.2. *Influence of temperature and CO_2 partial pressure*

Fig. 19 shows an Arrhenius plot for mixed gasification of P1400 and P1600 using CO_2 and H_2O partial pressures of 0.8 bar, respectively. Total pressure was constant at 5 bar while reaction temperatures were varied between 810 °C and 850 °C. During mixed gasification at $p_{H_2O} = p_{CO_2} = 0.8$ bar and a total pressure of 5 bar, P1600 showed a higher reactivity than P1400 within the temperature range investigated. Activation energies for these conditions can be taken from Table 10, being very similar to the values determined for single H_2O gasification at $p_{H_2O} = 0.8$ bar. According to Ergun [52], the strongly temperature dependent desorption of the C(O) surface complex (see Eqs. (R3) and (R6)) is the rate limiting step during heterogeneous gasification reaction. Thus, one possible explanation for the similar activation energies during mixed and pure H_2O gasification could be that the desorption rate of the C(O) complex originating from CO_2 gasification (see Eq. (R3)) is significantly lower than desorption of the C(O) complex from H_2O reaction (see Eq. (R6)). This would also indicate that CO_2 and H_2O gasification reaction takes place at different carbon active sites C_f for the bio-chars and process conditions investigated.

Fig. 20A shows the reaction rates r_{mix} as a function of CO_2 partial pressure in the range of 0 bar to 5 bar for H_2O partial pressures of 0.8 and 2 bar, respectively. In addition, one set of experimental data is reported for $p_{CO_2} = p_{H_2O} = 5$ bar. Temperature was constant at 830 °C for all experiments. Total pressure varied between 5 and 20 bar, however, the effect of total pressure on reactivity can be neglected, as shown in Sections 3.1.3 and 3.2.3. The values for $p_{CO_2} = 0$ bar correspond to the H_2O gasification experiments reported in Section 3.2.

As already shown in Section 3.2, P1400 shows a higher reactivity

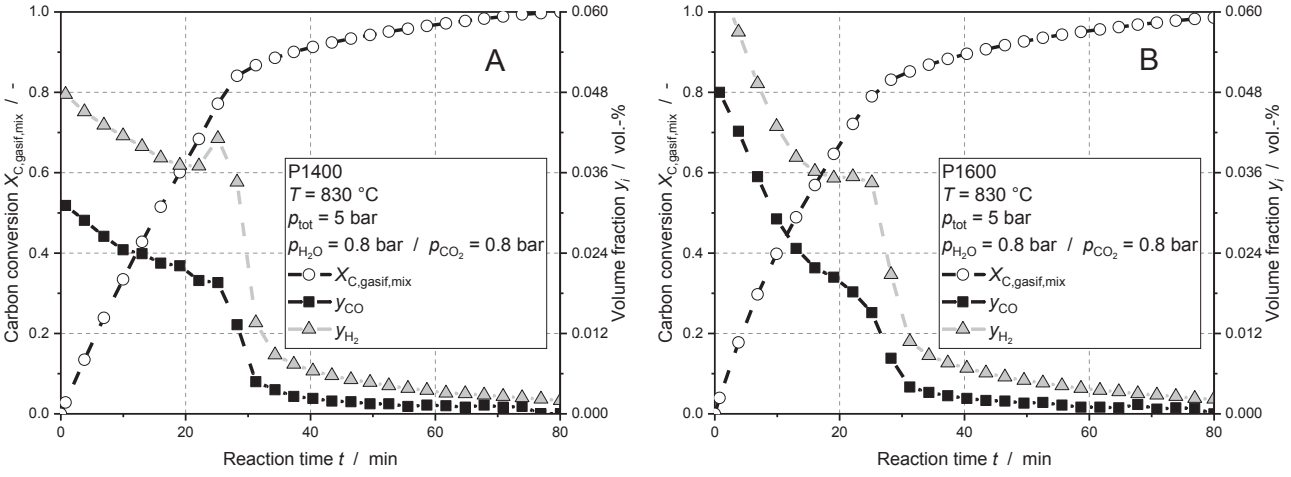

Fig. 18. CO volume fraction y_{CO}, H_2 volume fraction y_{H_2} and carbon conversion $X_{C,gasif,mix}$ during mixed gasification of P1400 (A) and P1600 (B) with H_2O and CO_2 at 830 °C ($p_{H_2O} = p_{CO_2} = 0.8$ bar, $p_{tot} = 5$ bar, diluting gas: argon).

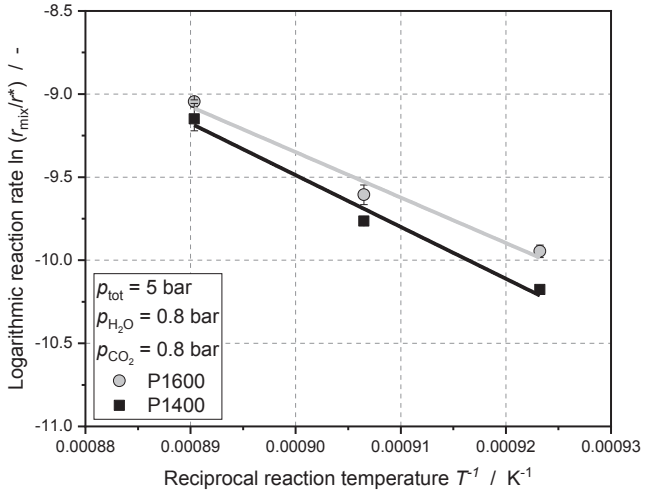

Fig. 19. Arrhenius plot for the gasification of P1400 and P1600 in a mixture of H_2O and CO_2 ($p_{H_2O} = p_{CO_2} = 0.8$ bar, $p_{tot} = 5$ bar and $T = 810–850$ °C, diluting gas: argon).

Table 10
Activation energies for mixed as well as pure H_2O and CO_2 gasification (both for $p_{H_2O} = 0.8$ bar) of P1400 and P1600.

		P1400	P1600
$E_{A,mix}$	kJ mol^{-1}	259.1	227.3
E_{A,H_2O}	kJ mol^{-1}	263.6	234.8
E_{A,CO_2}	kJ mol^{-1}	308.7	300.7

during gasification with H_2O ($p_{CO_2} = 0$ bar) as compared to P1600. For a CO_2 partial pressure of 0.8 bar, an increase in reaction rate r_{mix} for both chars at both H_2O partial pressure levels ($p_{H_2O} = 0.8$ bar and 2 bar) is detected. However, P1600 exhibits a stronger increase in reaction rate as compared to P1400 and becomes more reactive than P1400. For $p_{H_2O} = 0.8$ bar, both chars show a similar slope with increasing CO_2 partial pressure i.e. P1600 reactivity remains higher than P1400 reactivity. For $p_{H_2O} = 2$ bar, P1600 reaction rate r_{mix} remains almost constant for $p_{CO_2} > 0.8$ bar, whereas P1400 reactivity increases with CO_2 partial pressures at the same slope as for $p_{H_2O} = 0.8$ bar leading to a slightly higher reactivity at $p_{CO_2} = 5$ bar. At $p_{CO_2} = p_{H_2O} = 5$ bar, P1400 exhibits a significantly higher reaction rate r_{mix} as compared to P1600, which shows only a small increase in reactivity with increasing H_2O partial pressure from 2 bar to 5 bar.

Increasing the CO_2 partial pressure from 0 bar to 0.8 bar during mixed gasification leads to an increase in reaction rate r_{mix} for both chars which can be expressed by the addition of the single atmosphere reaction rates r_{CO_2} and r_{H_2O}. In Fig. 20B, the reaction rates r_{H_2O} and r_{CO_2} for single atmosphere gasification experiments at $p_{H_2O} = 0.8$ bar, 2 bar and $p_{CO_2} = 1$ bar, 5 bar are shown together with calculated values for r_{mix} using a simple addition of the single atmosphere reaction rates ($r_{mix} = r_{CO_2} + r_{H_2O}$). By this approach, the reaction rates for mixed gasification are reasonably modeled for the low pressure range up to $p_{CO_2} = 1$ bar and both chars, despite the fact that the experimental values are slightly overestimated for P1400. Thus, no competition between the H_2O and the CO_2 gasification reaction is observed in the low pressure range. Here, a separate active site mechanism might be valid for both chars. The strong increase of P1600 reactivity from $p_{CO_2} = 0$ bar to $p_{CO_2} = 0.8$ bar may be explained by the catalytic activity of the CaO film on the char surface selectively increasing the reactivity towards CO_2 (see Section 3.1).

At $p_{H_2O} = 2$ bar, however, the reaction rate r_{mix} of P1600 stagnates for CO_2 partial pressures above 0.8 bar (see Fig. 20A). The observed trend may be interpreted as saturation of reactant gases on the char surface since P1600 has a distinctly lower surface area as P1400 and – due to a higher graphitization degree – a lower amount of carbon active sites. Thus, morphology and graphitization might become more relevant for higher reactant gas partial pressures while Ca catalysis fades into the background. At high reactant gas partial pressures, a common reactive sites mechanism might be more adequate for P1600. Here, the simple addition of the single atmosphere reaction rates might become invalid. This thesis is fortified by the experimental results at $p_{CO_2} = p_{H_2O} = 5$ bar, where an inhibition of the P1600 reactivity is clearly visible as compared to P1400.

3.3.3. Reaction kinetic modeling

Experimental results from the previous chapter indicate that – for the chars and process conditions investigated – CO_2 and H_2O gasification occurs rather on separate than on same active sites except for the high pressure experiments with P1600. Therefore, simple approaches were used in order to model mixed gasification via addition of the single atmosphere reaction kinetics with the highest fit quality (see Sections 3.1.4 and 3.2.4). For pressurized CO_2 gasification, the power law approach was most suitable for P1400 while LH represented the

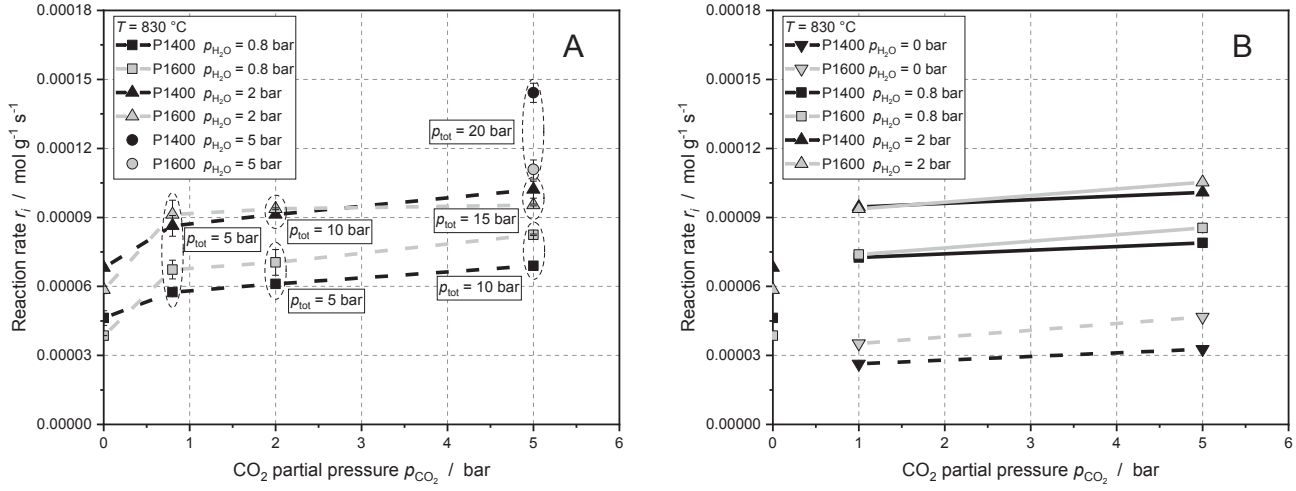

Fig. 20. (A) Reaction rates r_{mix} of P1400 and P1600 during mixed gasification at 830 °C for three H_2O partial pressures ($p_{H_2O} = 0.8$ bar, 2 bar, 5 bar and $p_{tot} = 5 – 20$ bar) as a function of p_{CO_2} as well as r_{H_2O} at $p_{H_2O} = 0.8$ bar, 2 bar. (B) Reaction rates r_{H_2O} and r_{CO_2} for single atmosphere gasification experiments at $p_{H_2O} = 0.8$ bar, 2 bar and $p_{CO_2} = 1$ bar, 5 bar; r_{mix} plotted as a simple addition of the single atmosphere reaction rates (symbols with solid line).

characteristics of P1600 very well especially in the high pressure range. In terms of H_2O gasification, both chars could be sufficiently modeled using the power law approach taking into account the lower reactant gas partial pressures investigated.

Fig. 21A shows the experimental reaction rates of P1400 for CO_2, H_2O and mixed atmosphere gasification together with the corresponding modeling approaches. Promoting a better understanding of the diagram, it is necessary to illustrate the reading of the axis of abscissae: Concerning mixed atmosphere gasification (black dots), both reactant gases had the same partial pressure i.e. $p_{H_2O} = p_{CO_2} = 0.8$ bar, 2 bar and 5 bar. The black line represents the model for mixed atmosphere gasification of P1400 calculated by an addition of both single atmosphere power laws. The remaining experimental values (grey boxes and triangles) are the reaction rates for single atmosphere gasification with the corresponding H_2O or CO_2 partial pressures, respectively.

The simple addition of the single atmosphere reaction kinetics gives a satisfying modeling of the mixed atmosphere gasification reaction for P1400 (see Fig. 21A). The experimental values are rather overestimated by the addition of the single atmosphere reaction kinetics. However, the conception of a separate carbon active sites reaction mechanism is significantly better represented as compared to the approach of same active sites, which is calculated according to the following LH based approach [53]:

$$r_{mix}\left(T, p_{H_2O}, p_{CO_2}\right) = \frac{k_1 p_{CO_2} + k_4 p_{H_2O}}{1 + \frac{k_1}{k_3} p_{CO_2} + \frac{k_4}{k_6} p_{H_2O}} \quad (27)$$

These findings correspond well with the results of Chen et al. [17] who gasified two lignite chars in mixed CO_2/H_2O atmospheres using TGA and fluidized bed. They reported that the gasification rate in CO_2/H_2O mixtures was lower than the sum of both rates but higher than the rate of each independent gasification reaction. Furthermore, the authors stated that char-H_2O reaction was independent from char-CO_2 reaction, what could also be observed for the experiments in the present work (see Section 3.3.2).

Fig. 21B shows the corresponding diagram for mixed atmosphere gasification of P1600. Here, the model approach is conducted using the addition of CO_2 LH kinetics and H_2O power law, since these approaches gave the best quality of fit for the char sample. In contrast to P1400, the addition of both single atmosphere kinetics only gives a satisfying modeling for reactant gas partial pressures up to $p_{H_2O} = p_{CO_2} = 2$ bar. It was already depicted in Fig. 20A (see Section 3.3.2) that the char surface of P1600 reaches a state of saturation applying high pressures resulting in a stagnation of r_{mix}. This phenomenon can also be seen in Fig. 21B at $p_{H_2O} = p_{CO_2} = 5$ bar where the addition of both single atmosphere kinetics becomes invalid and a saturation of the char surface can be assumed. These results also correspond well with the results of Li et al. [22] who gasified lignite with H_2O, CO_2 and its mixtures in a pressurized fixed bed reactor which is similar to the system used in this work. The authors reported that the separate active sites mechanism is valid for relatively low pressures. Moreover, their results indicate that the common active site mechanism becomes relevant applying higher reactant gas partial pressures.

Considering the results presented in this work, this thesis can be expanded in terms of high pressures and specific surface area and graphitization degree. For bio-chars with a rather low specific surface area and fewer carbon active sites – as it is the case for P1600 – a separate active site reaction mechanism is only valid in the low pressure range (up to $p_{H_2O} = p_{CO_2} = 2$ bar in the present work). In contrast to P1400, the char surface of P1600 shows a saturation applying high pressures where a common active site mechanism can be assumed. However, more mixed atmosphere experiments need to be conducted – especially in the high reactant gas partial pressure area – in order to further verify this thesis.

4. Summary and conclusions

The objective of the present work was to investigate the influence of pressure on the gasification kinetics for two beech wood chars that were produced at 1400 °C and 1600 °C at high-heating rates and short residence times in a drop-tube reactor. The gasification experiments presented in this work were conducted in a single-particle reactor with forced flow-through conditions reducing diffusional effects to a minimum. The interpretation of the experimentally determined reaction rates during gasification with CO_2, H_2O and its mixture is based on the char properties (graphitization, ash dispersion and morphology) presented in a previous publication [32]. Kinetic parameters for the gasification of both beech wood chars (P1400 and P1600) with CO_2 and H_2O at elevated pressure were derived using an nth-order and a Langmuir-Hinshelwood (LH) approach. Furthermore, gasification experiments in a mixture of CO_2 and H_2O were carried out in order to further clarify the dominating reaction mechanism during gasification of biomass chars in CO_2/H_2O containing atmospheres. A possible approach for the reaction kinetic modeling in mixtures of CO_2 and H_2O is presented for both biochars.

Dominating char properties affecting gasification reactivity with CO_2 and H_2O were found to be (i) specific surface area, (ii) graphitization degree and (iii) dispersion of catalytic ash components. Due to the higher pyrolysis temperature of P1600, this char showed a higher graphitization degree (lower amount of carbon active sites) and a lower specific surface area as compared to P1400. Furthermore, a thin

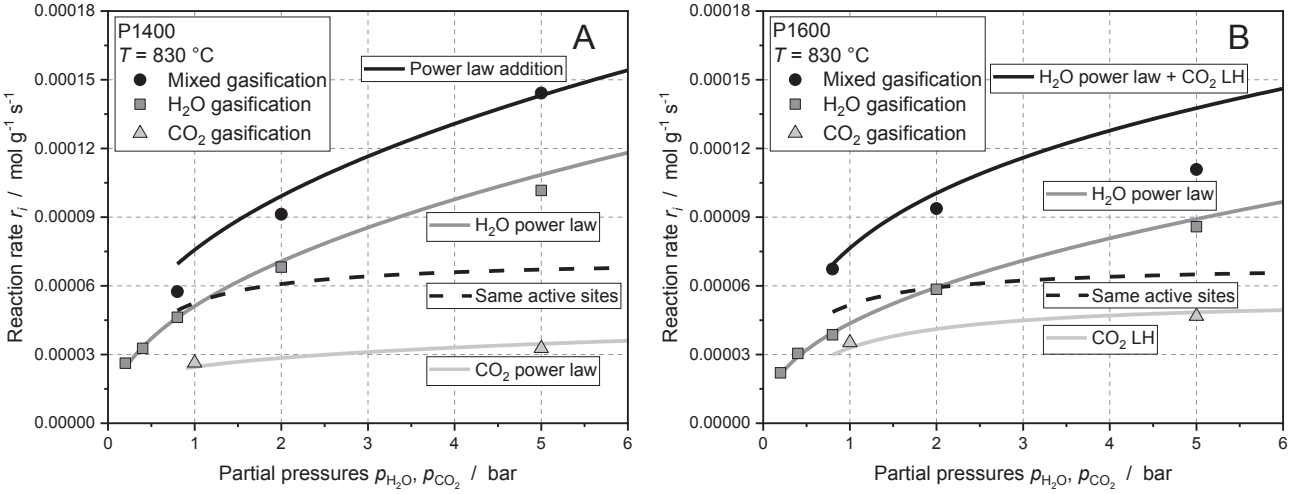

Fig. 21. Modeling approaches for the mixed H_2O/CO_2 gasification of P1400 (A) and P1600 (B) using an addition of the single atmosphere reaction kinetics.

catalytically active CaO layer formed on the surface of P1600 leading to an increased reactivity towards CO_2 [32].

4.1. Gasification with CO_2

P1600 shows higher reactivity as compared to P1400 for all CO_2 partial pressures and temperatures applied. However, for the highest CO_2 partial pressure applied (20 bar), both chars show similar reactivity. The higher reactivity of P1600 during CO_2 gasification may be explained by the CaO film on the char surface catalyzing the char-CO_2 gasification reaction [32]. A power law approach is suitable to describe gasification kinetics of both chars with CO_2 up to pressures of 20 bar. However, the observed saturation during gasification of P1600 applying high CO_2 partial pressures is better described by a LH approach.

4.2. Gasification with H_2O

P1400 shows higher reactivity towards H_2O as compared to P1600 which is expected from the char specifications reported above. The dominating char properties affecting H_2O reactivity were considered to be constitution of carbon matrix (i.e. graphitization degree) and micropore surface area. The catalytically active CaO film is of minor relevance when gasification is carried out with H_2O. Modeling of pressurized char-H_2O gasification kinetics of both samples was achieved using a power law approach to full satisfaction within the process conditions applied.

4.3. Gasification in mixed CO_2/H_2O atmosphere

Increasing the CO_2 partial pressure from 0 bar to 0.8 bar during mixed gasification leads to an increase in reaction rate r_{mix} for both chars which can be expressed by the addition of the single atmosphere reaction rates r_{CO_2} and r_{H_2O}. Thus, no competition between the H_2O and the CO_2 gasification reaction is observed in this low pressure range. Here, a separate active site mechanism might be valid for both chars. The strong increase of P1600 reactivity from $p_{CO_2} = 0$ bar to $p_{CO_2} = 0.8$ bar may be explained by the catalytic activity of the CaO film on the char surface selectively increasing the reactivity towards CO_2. At $p_{H_2O} = 2$ bar, the reaction rate r_{mix} of P1600 stagnates for CO_2 partial pressures above 0.8 bar. The observed trend may be interpreted as saturation of reactant gases on the char surface since P1600 has a distinctly lower surface area as P1400 and – due to a higher graphitization degree – a lower amount of carbon active sites. Thus, morphology and graphitization might become more relevant for higher reactant gas partial pressures while Ca catalysis fades into the background. At high reactant gas partial pressures, a common reactive sites mechanism might be more adequate for P1600. This thesis is fortified by the experimental results at $p_{CO_2} = p_{H_2O} = 5$ bar, where an inhibition of the P1600 reactivity is clearly visible as compared to P1400.

Concerning a possible modeling approach for mixed gasification, the addition of the single atmosphere reaction kinetics gives satisfying results for P1400. The experimental values are slightly overestimated by the addition of the single atmosphere reaction kinetics. However, the conception of a separate carbon active sites reaction mechanism is significantly better represented as compared to the approach of competing active sites.

In contrast to P1400, the addition of both single atmosphere kinetics of P1600 for modeling of mixed gasification gives satisfying results only in the low pressure range. The char with the lower specific surface area and the higher graphitization degree (P1600) reaches a saturated state earlier when applying higher reactant gas partial pressures. Therefore, the addition of both single atmosphere kinetics becomes invalid and a common active site mechanism might be relevant.

Considering the experimental results for mixed gasification presented in this work, the following conclusions can be drawn:

- Increasing the CO_2 partial pressure during mixed gasification leads to higher reactivity for both chars. The reaction rate r_{mix} can be expressed by addition of the single atmosphere reaction rates in the low pressure area suggesting a separate active site mechanism.
- Catalytic activity of CaO increases the reaction rate r_{mix} of P1600 distinctively for lower H_2O and CO_2 partial pressures.
- For higher H_2O and CO_2 partial pressures, P1600 reactivity stagnates due to lower specific surface area and higher graphitization degree i. e. lower amount of carbon active sites. Here, a common active sites mechanism can be assumed.

5. Glossary

Symbol	Description	Unit
a, b, c	Global reaction rates for mixed CO_2/H_2O gasification	mol s^{-1}
D_{AB}	Binary diffusion coefficient	m^2 s^{-1}
D_{CaO}	Dispersion of superficial calcium oxide	mol g^{-1}
$\frac{dX}{dt}$	Conversion rate	s^{-1}
E_A	Activation energy	kJ mol^{-1}
$F(X_C)$	Structural term	–
k_0	Pre-exponential factor	s^{-1} bar^{-n}
L_a	Radial expansion of graphene layers	m
$L_{a,0}$	Radial expansion of graphene layers of primary char	m
k_j	Arrhenius rate coefficient	Various
M_C	Molar mass of carbon	g mol^{-1}
$m_{C,gasif}$	Gasified mass of carbon	g
$m_{C,0}$	Initial mass of fixed carbon	g
$m_C(t)$	Remaining carbon mass at a certain time t	g
m_{char}	Char mass	g
m_{Sample}	Sample mass	g
n	Reaction order	–
$\dot{n}$	Molar flow rate	mol s^{-1}
$\dot{n}_{C,out}$	Molar flow rate of carbon containing gasification product gases	mol s^{-1}
$\dot{n}_{out}$	Molar flow rate of gasification product gases	mol s^{-1}
p	System pressure	bar
p_i	Partial pressure of component i	bar
p_{tot}	Total pressure	bar
$R(T,p)$	Chemical rate coefficient	s^{-1}
R_0	Initial conversion rate	s^{-1}
R_U	Universal gas constant	J mol^{-1} K^{-1}
R_X	Conversion rate	s^{-1}
r^*	Dummy reaction rate ($r^* = 1$ mol g^{-1} s^{-1})	mol g^{-1} s^{-1}
r_i	Reaction rate ($i = CO_2$, H_2O, mix)	mol g^{-1} s^{-1}
T	Temperature	K
t	Time	s
v_{gas}	Superficial linear gas velocity	m s^{-1}
V	Volume	m^3
$\dot{V}$	Volume flow rate	m^3 s^{-1}
V	Molar volume	m^3 mol^{-1}
X_C	Carbon conversion	–
$x_{C,fix}$	Mass fraction of fixed carbon	–
y_i	Volume fraction of component i	–
y_i	Molar fraction of component i	–

Subscripts	Description
C	Carbon
C,fix	Fixed Carbon
CO	Carbon monoxide molecule
CO_2	Concerning CO_2 gasification
end	End of experiment
f	Fixed carbon (in chemical reaction equation)
gasif	Gasified
H_2	Hydrogen molecule
H_2O	Concerning H_2O gasification
i	Control variable
j	Control variable
mix	Concerning mixed gasification in CO_2/H_2O atmosphere
N_2	Nitrogen molecule
surface-CaO	Superficial calcium oxide

Abbreviations	Description
ad	Air-dried
BY	Bypass
CEM	Controlled evaporation and mixing unit
CORI	Coriolis flow controller
daf	Dry ash free
DFG	Deutsche Forschungsgemeinschaft
diff	Determined by difference
EMR	Energy, materials and resources
EFG	Entrained-flow gasification
Eq.	Equation
Fig.	Figure
GC	Gas chromatograph
HGF	Helmholtz-Gemeinschaft Deutscher Forschungszentren
ICP-OES	Inductively coupled plasma optical emission spectrometry
IGCC	Integrated Gasification Combined Cycle
IR	Infrared spectroscopy
KIT	Karlsruhe Institute of Technology
LH	Langmuir-Hinshelwood
MFC	Mass flow controller
P1400, P1600	Chars produced at 1400 °C and 1600 °C
ppm	Parts per million
PTFE	Polytetrafluoroethylene
SEM	Scanning electron microscope
TEM	Transmission electron microscope
TGA	Thermogravimetric analyzer
TPR	Temperature-programmed reaction
UCM	Uniform Conversion Model
vol.	Volume
WGS	Water-gas shift reaction
wt.	Weight
XRD	X-ray diffraction

CRediT authorship contribution statement

Christoph Schneider: Conceptualization, Methodology, Validation, Investigation, Data curation, Writing - original draft, Visualization, Supervision, Project administration. **Michael Zeller:** Methodology, Validation, Investigation, Data curation, Writing - review & editing, Visualization. **Daniel Böhm:** Methodology, Validation, Investigation, Data curation, Writing - review & editing, Visualization. **Thomas Kolb:** Resources, Writing - review & editing, Supervision.

Declaration of Competing Interest

The authors declare that they have no known competing financial interests or personal relationships that could have appeared to influence the work reported in this paper.

Acknowledgments

The authors gratefully acknowledge the financial support by the Deutsche Forschungsgemeinschaft (DFG) (121384/22-1) and the Helmholtz Association of German Research Centers (HGF), within the research program Energy Efficiency, Materials and Resources (EMR). The present work contributes to the Helmholtz Virtual Institute for Gasification Technology - HVIGasTech (VH-VI-429, http: //www.hvi-gastech.org/).

Appendix A. Supplementary data

Supplementary data associated with this article can be found, in the online version, at https://doi.org/10.1016/j.fuel.2021.120523.

References

[1] Dahmen N, Abeln J, Eberhard M, Kolb T, Leibold H, Sauer J, et al. The bioliq process for producing synthetic transportation fuels. WIREs Energy Environ 2017;6 (3). https://doi.org/10.1002/wene.236.
[2] Higman C, others. State of the gasification industry-the updated worldwide gasification database. In: Gasification Technology Conference, Colorado Springs; 2013.
[3] Kolb T, Aigner M, Kneer R, Müller M, Weber R, Djordjevic N. Tackling the challenges in modelling entrained-flow gasification of low-grade feedstock. J Energy Inst 2016;89(4):485–503. https://doi.org/10.1016/j.joei.2015.07.007.
[4] Liu G-S, Niksa S. Coal conversion submodels for design applications at elevated pressures. Part II. Char gasification. Prog Energy Combust Sci 2004;30(6):679–717. https://doi.org/10.1016/j.pecs.2004.08.001.
[5] Lu L. Char structural ordering during pyrolysis and combustion and its influence on char reactivity. Fuel 2002;81(9):1215–25. https://doi.org/10.1016/S0016-2361(02)00035-2.
[6] Lobo LS, Carabineiro SAC. Kinetics and mechanism of catalytic carbon gasification. Fuel 2016;183:457–69. https://doi.org/10.1016/j.fuel.2016.06.115.
[7] Bai J, Li W, Li C-z, Bai Z, Li B. Influences of minerals transformation on the reactivity of high temperature char gasification. Fuel Process Technol 2010;91(4): 404–9. https://doi.org/10.1016/j.fuproc.2009.05.017.
[8] Wang Y-L, Zhu S-H, Gao M-Q, Yang Z-R, Yan L-J, Bai Y-H, et al. A study of char gasification in H2O and CO2 mixtures: Role of inherent minerals in the coal. Fuel Process Technol 2016;141:9–15. https://doi.org/10.1016/j.fuproc.2015.06.001.
[9] Laurendeau NM. Heterogeneous kinetics of coal char gasification and combustion. Prog Energy Combust Sci 1978;4(4):221–70. https://doi.org/10.1016/0360-1285(78)90008-4.
[10] Blackwood JD, Ingeme AJ. The reaction of carbon with carbon dioxide at high pressure. Aust J Chem 1960;13(2):194. https://doi.org/10.1071/CH9600194.
[11] Roberts DG, Harris DJ. A kinetic analysis of coal char gasification reactions at high pressures. Energy Fuels 2006;20(6):2314–20. https://doi.org/10.1021/ef060270o.
[12] Hüttinger KJ, Merdes WF. The carbon-steam reaction at elevated pressure: Formations of product gases and hydrogen inhibitions. Carbon 1992;30(6):883–94. https://doi.org/10.1016/0008-6223(92)90011-K.
[13] Barrio M, Gøbel B, Risnes H, Henriksen UB, Hustad JE, Sørensen LH. Steam gasification of wood char and the effect of hydrogen inhibition on the chemical kinetics. In: Conference on progress in thermochemical biomass conversion; 2000.
[14] Roberts DG, Harris DJ. Char gasification in mixtures of CO2 and H2O: Competition and inhibition. Fuel ;86(17–18):2672–8. https://doi.org/10.1016/j.fuel.2007.03.019.
[15] Goyal A, Zabransky RF, Rehmat A. Gasification kinetics of Western Kentucky bituminous coal char. Ind Eng Chem Res 1989;28(12):1767–78. https://doi.org/10.1021/ie00096a006.
[16] Mühlen H-J, van Heek KH, Jüntgen H. Kinetic studies of steam gasification of char in the presence of H2, CO2 and CO. Fuel 1985;64(7):944–9. https://doi.org/10.1016/0016-2361(85)90149-8.
[17] Chen C, Wang J, Liu W, Zhang S, Yin J, Luo G et al. Effect of pyrolysis conditions on the char gasification with mixtures of CO2 and H2O. Proceedings of the Combustion Institute 2013;34(2):2453–60. doi:10.1016/j.proci.2012.07.068.
[18] Chen C, Zhang S, Xu K, Luo G, Yao H. Experimental and Modeling Study of Char Gasification with Mixtures of CO2 and H2O. Energy Fuels 2015;30(3):1628–35. https://doi.org/10.1021/acs.energyfuels.5b02294.
[19] Huang Z, Zhang J, Zhao Y, Zhang H, Yue G, Suda T, et al. Kinetic studies of char gasification by steam and CO2 in the presence of H2 and CO. Fuel Process Technol 2010;91(8):843–7. https://doi.org/10.1016/j.fuproc.2009.12.020.
[20] Everson RC, Neomagus HWJP, Kasaini H, Njapha D. Reaction kinetics of pulverized coal-chars derived from inertinite-rich coal discards: Gasification with carbon dioxide and steam. Fuel 2006;85(7–8):1076–82. https://doi.org/10.1016/j.fuel.2005.10.016.
[21] Guizani C, Escudero Sanz FJ, Salvador S. Influence of temperature and particle size on the single and mixed atmosphere gasification of biomass char with H2O and CO2. Fuel Process Technol 2015;134:175–88. https://doi.org/10.1016/j.fuproc.2015.01.031.
[22] Li F, Yan Q, Huang J, Zhao J, Fang Y, Wang J. Lignite-char gasification mechanism in mixed atmospheres of steam and CO2 at different pressures. Fuel Process Technol 2015;138:555–63. https://doi.org/10.1016/j.fuproc.2015.06.035.
[23] Guizani C, Escudero Sanz FJ, Salvador S. The gasification reactivity of high-heating-rate chars in single and mixed atmospheres of H2O and CO2. Fuel 2013; 108:812–23. https://doi.org/10.1016/j.fuel.2013.02.027.
[24] Irfan MF, Usman MR, Kusakabe K. Coal gasification in CO2 atmosphere and its kinetics since 1948: A brief review. Energy 2011;36(1):12–40. https://doi.org/10.1016/j.energy.2010.10.034.
[25] Di Blasi C. Combustion and gasification rates of lignocellulosic chars. Prog Energy Combust Sci 2009;35(2):121–40. https://doi.org/10.1016/j.pecs.2008.08.001.
[26] Senneca O, Salatino P, Masi S. Microstructural changes and loss of gasification reactivity of chars upon heat treatment. Fuel 1998;77(13):1483–93. https://doi.org/10.1016/S0016-2361(98)00056-8.
[27] Senneca O, Apicella B, Russo C, Cerciello F, Salatino P, Heuer S, et al. Pyrolysis and thermal annealing of coal and biomass in CO2-rich atmospheres. Energy Fuels 2018;32(10):10701–8. https://doi.org/10.1021/acs.energyfuels.8b02417.
[28] Tremel A, Spliethoff H. Gasification kinetics during entrained flow gasification – Part I Devolatilisation and char deactivation. Fuel 2013;103:663–71. https://doi.org/10.1016/j.fuel.2012.09.014.

[29] Cetin E, Moghtaderi B, Gupta R, Wall TF. Influence of pyrolysis conditions on the structure and gasification reactivity of biomass chars. Fuel 2004;83(16):2139–50. https://doi.org/10.1016/j.fuel.2004.05.008.
[30] Radovic LR, Steczko K, Walker PL, Jenkins RG. Combined effects of inorganic constituents and pyrolysis conditions on the gasification reactivity of coal chars. Fuel Process Technol 1985;10(3):311–26. https://doi.org/10.1016/0378-3820(85)90038-4.
[31] Cazorla-Amoros D, Linares-Solano A, Salinas-Martinez de Lecea C, Nomura M, Yamashita H, Tomita A. Local structure of calcium species dispersed on carbon: Influence of the metal loading procedure and its evolution during pyrolysis. Energy Fuels 1993;7(5):625–31. https://doi.org/10.1021/ef00041a010.
[32] Schneider C, Walker S, Phounglamcheik A, Umeki K, Kolb T. Effect of calcium dispersion and graphitization during high-temperature pyrolysis of beech wood char on the gasification rate with CO2. Fuel 2021;283. https://doi.org/10.1016/j.fuel.2020.118826.
[33] Ollero P. Diffusional effects in TGA gasification experiments for kinetic determination. Fuel 2002;81(15):1989–2000. https://doi.org/10.1016/S0016-2361(02)00126-6.
[34] Nowak B, Karlström O, Backman P, Brink A, Zevenhoven M, Voglsam S, et al. Mass transfer limitation in thermogravimetry of biomass gasification. J Therm Anal Calorim 2013;111(1):183–92. https://doi.org/10.1007/s10973-012-2400-9.
[35] Stoesser P, Schneider C, Kreitzberg T, Kneer R, Kolb T. On the influence of different experimental systems on measured heterogeneous gasification kinetics. Appl Energy 2018;211:582–9. https://doi.org/10.1016/j.apenergy.2017.11.037.
[36] Wu X, Wang J. K2CO3-catalyzed steam gasification of ash-free coal char in a pressurized and vertically blown reactor. Influence of pressure on gasification rate and gas composition. Fuel Process Technol 2017;159:9–18. https://doi.org/10.1016/j.fuproc.2017.01.001.
[37] Bouraoui Z, Dupont C, Jeguirim M, Limousy L, Gadiou R. CO2 gasification of woody biomass chars: the influence of K and Si on char reactivity. C R Chim 2016;19(4):457–65. https://doi.org/10.1016/j.crci.2015.08.012.
[38] Dupont C, Nocquet T, Da Costa JA, Verne-Tournon C. Kinetic modelling of steam gasification of various woody biomass chars: influence of inorganic elements. Bioresour Technol 2011;102(20):9743–8. https://doi.org/10.1016/j.biortech.2011.07.016.
[39] Linares-Solano A, Almela-Alarcón M, Lecea CS-Md. CO2 chemisorption to characterize calcium catalysts in carbon gasification reactions. J Catal 1990;125(2):401–10. https://doi.org/10.1016/0021-9517(90)90313-9.
[40] Laine NR, Vastola FJ, Walker Jr PL. The importance of active surface area in the carbon-oxygen reaction. J Phys Chem 1963;67(10):2030–4.
[41] Levenspiel O. The chemical reactor omnibook. 5th ed. Corvallis, Or: OSU Book Stores Inc; 1996.
[42] P. W. J. Struis R, Scala C von, Stucki S, Prins R. Gasification reactivity of charcoal with CO2. Part II: Metal catalysis as a function of conversion. Chemical Engineering Science 2002;57(17):3593–602. doi:10.1016/S0009-2509(02)00255-5.
[43] Cazorla-Amoros D, Linares-Solano A, Salinas-Martinez de Lecea C, Yamashita H, Kyotani T, Tomita A, et al. XAFS and thermogravimetry study of the sintering of calcium supported on carbon. Energy Fuels 1993;7(1):139–45.
[44] Fermoso J, Stevanov C, Moghtaderi B, Arias B, Pevida C, Plaza MG, et al. High-pressure gasification reactivity of biomass chars produced at different temperatures. J Anal Appl Pyrol 2009;85(1–2):287–93. https://doi.org/10.1016/j.jaap.2008.09.017.
[45] Cetin E, Moghtaderi B, Gupta R, Wall TF. Biomass gasification kinetics: influences of pressure and char structure. Combust Sci Technol 2006;177(4):765–91. https://doi.org/10.1080/00102200590917266.
[46] Li C, Zhao J, Fang Y, Wang Y. Effect of pressure on gasification reactivity of three Chinese coals with different ranks. Front Chem Eng China 2010;4(4):385–93. https://doi.org/10.1007/s11705-010-0501-1.
[47] Sander R. Compilation of Henry's law constants (version 4.0) for water as solvent. Atmos Chem Phys 2015;15(8):4399–981.
[48] Elstner M. Physikalische Chemie I: Thermodynamik und Kinetik. Berlin, Heidelberg: Springer Spektrum; 2017.
[49] Yan Q, Huang J, Zhao J, Li C, Xia L, Fang Y. Investigation into the kinetics of pressurized steam gasification of chars with different coal ranks. J Therm Anal Calorim 2014;116(1):519–27. https://doi.org/10.1007/s10973-013-3492-6.
[50] Roberts DG, Harris DJ. Char Gasification with O2, CO2, and H2O: effects of pressure on intrinsic reaction kinetics. Energy Fuels 2000;14(2):483–9. https://doi.org/10.1021/ef9901894.
[51] Matsuoka K, Kajiwara D, Kuramoto K, Sharma A, Suzuki Y. Factors affecting steam gasification rate of low rank coal char in a pressurized fluidized bed. Fuel Process Technol 2009;90(7–8):895–900. https://doi.org/10.1016/j.fuproc.2009.04.001.
[52] Ergun S. Kinetics of the reactions of carbon dioxide and steam with coke. US Government Printing Office 1962.
[53] Wang Y, Bell DA. Competition between H2O and CO2 during the gasification of Powder River Basin coal. Fuel 2017;187:94–102. https://doi.org/10.1016/j.fuel.2016.08.109.